

PCCP

Accepted Manuscript



This is an *Accepted Manuscript*, which has been through the Royal Society of Chemistry peer review process and has been accepted for publication.

Accepted Manuscripts are published online shortly after acceptance, before technical editing, formatting and proof reading. Using this free service, authors can make their results available to the community, in citable form, before we publish the edited article. We will replace this *Accepted Manuscript* with the edited and formatted *Advance Article* as soon as it is available.

You can find more information about *Accepted Manuscripts* in the [Information for Authors](#).

Please note that technical editing may introduce minor changes to the text and/or graphics, which may alter content. The journal's standard [Terms & Conditions](#) and the [Ethical guidelines](#) still apply. In no event shall the Royal Society of Chemistry be held responsible for any errors or omissions in this *Accepted Manuscript* or any consequences arising from the use of any information it contains.

Ultrafast solvation dynamics and charge transfer reactions in room temperature ionic liquids

Yutaka Nagasawa^{1-3} and Hiroshi Miyasaka^{1,2*}*

¹ Division of Frontier Materials Science, Department of Materials Engineering Science, Graduate School of Engineering Science, Osaka University, Toyonaka, Osaka 560-8531, Japan

² Center for Quantum Science and Technology under Extreme Conditions, Osaka University, Toyonaka, Osaka 560-8531, Japan

³ PRESTO, Japan Science and Technology Agency (JST), Kawaguchi, Saitama 332-0012, Japan

nagasawa@chem.es.osaka-u.ac.jp

miyasaka@chem.es.osaka-u.ac.jp

RECEIVED DATE

Abstract

Room temperature ionic liquid (IL) is a new type of solvent with peculiar properties. IL is usually composed of an anion and a bulky cation with one or more alkyl chains to decrease the melting point. These structural peculiarities lead to the high viscosity and the heterogeneity of IL, which could affect chemical reactions. In the present perspective, we will first introduce the experimentally observed nature of the heterogeneous liquid structure and then introduce recent developments in the study on electron transfer (ET) and charge transfer (CT) reactions in relation with the solvation and the heterogeneity of IL. Because of the high viscosity of IL, diffusive solvation is expected to be slow which could be the rate limiting factor for ET and CT processes. However, IL could provide unique reaction field depending on the location of the solute within the heterogeneous liquid structure and the reaction could be faster than that expected from the bulk viscosity due to the fast fluctuation of the local environment.

1. Introduction

Room temperature ionic liquids (ILs), typical molecular structures of which are shown in Figure 1, are molten salts that possess peculiar properties such as high ionic conductivity, nearly zero vapor pressure, and inflammability, which make it an attractive new type of solvent.¹⁻¹⁴ Vast number of fundamental studies have been reported to thoroughly understand the physical characters of IL.¹⁵⁻²¹ While molecular structure of a normal polar solvent is rather rigid and the electric dipole moment is static, anions and cations of IL are mobile and the distance between the charges is variable in principle. Therefore, solvation shell formed by IL could be different from those of normal polar solvents, of which property could significantly affect chemical reactions accompanying charge redistribution. Moreover, ILs are known to be highly viscous and heterogeneous with microscopic segregation.²²⁻²⁸ Cations of IL usually possess bulky alkyl chains to prevent crystallization and to reduce the melting point. The weak nonpolar interaction between these alkyl chains induce aggregation and reverse micelle-like nonpolar region surrounded by ion-rich polar domain is formed.²⁹ It is confirmed by small-angle X-ray diffraction that the size of the domain is in the order of a few nanometers depending on the length of the alkyl chain.²² It is of great interest how chemical reaction is affected by such a liquid structure, which could be applied as a new type of reaction field.

It is well known that the rate constant of electron transfer (ET) and charge transfer (CT) depends on the energy gap between the reactant and product states and also on the inter- and intra-molecular reorganization energies.³⁰⁻³³ In the case of strongly coupled adiabatic reaction with the solvent reorganization (solvation) being the main driving force, solvation dynamics³⁴⁻³⁸ could be the rate limiting factor. ILs are usually highly viscous (≥ 50 cP) and their diffusive solvation process is much slower than those in normal organic solvents. Accordingly, the time constant for ET and CT is estimated to be quite slow, which could be an obstacle to the application of IL in a photon-energy conversion system, *i.e.*, to attain high efficiency, it is crucially important for the ET/CT reactions to occur within the finite lifetime of the electronically excited state.

Solvation dynamics and ET/CT reaction can be divided into several elementary processes which occur in variety of time scales from femtoseconds to hundreds of picoseconds. In viscous solvents, it is known that the solvation dynamics takes place in a hierarchic manner and the relaxation process is not monophasic. It is suggested for ILs that ions inside local structure can rattle very rapidly while reorganization of larger scale liquid structure occurs in a longer time scale.²⁸ The solvation dynamics in picosecond time scale and longer are diffusive which depend strongly on the viscosity of IL. On the other hand, the solvent response in the sub-picosecond range is known as "inertial" component which is independent of viscosity. In this ultrashort time scale where the number of collisions between the molecules is limited, solvent molecules in the vicinity of a solute can move quite freely for a microscopic angle which induces ultrafast solvation.^{36, 39, 40} Moreover, not only solvent reorganization but also intramolecular nuclear reorganization is known to contribute to CT which is expected to occur faster than the diffusive solvation.^{31, 41-43} Accordingly, ET/ CT could be initially induced by these ultrafast motions while the slow diffusive solvation process contributes to the stabilization of produced CT state in the final step.

In this perspective, we will review the recent studies concerning the liquid structure, the solvation dynamics of IL and their influence upon ET and CT reactions. The high viscosity of IL is considered to be a problem for efficient chemical reaction, however, IL could provide unique reaction field depending on the location of the solute within the heterogeneous liquid structure and the reaction could be faster than that expected from the bulk viscosity due to the fast fluctuation of the local environment.

2. Heterogeneity of Ionic liquid

The cations of IL usually possess bulky alkyl groups to prevent crystallization and to reduce the melting point. Hence, IL is comprised from a highly dipolar head group and a nonpolar tail. The weak nonpolar interaction between the alkyl chains induce aggregation and reverse micelle-like nonpolar domains are

formed which are surrounded by ion-rich polar domains induced by the Coulombic interaction between the ions.^{15, 29}

2.1. Observation by X-ray diffraction and predicted structure by MD simulations

Clear experimental evidence of the existence of nanoscale heterogeneities were obtained by small-angle X-ray diffractions in neat 1-alkyl-3-methylimidazolium and N-alkyl-N-methylpiperidinium ILs.^{22, 44-47} The heterogeneities are in the order of a few nanometers and their size linearly scaled with the number of carbon atoms, n , in the alkyl chain as shown in Figure 2.⁴⁸ The size of the spatial correlation is also temperature dependent and it increased with decreasing temperature until the glass transition point.

These heterogeneities were predicted also by molecular dynamics (MD) simulations.^{25, 26, 49, 50} Wang *et al.* performed MD simulation based on multiscale coarse-graining (MS-CG) model and they showed that, while the charged anions and head portion of the cations of IL distribute homogeneously because of the long-range Coulomb interactions, the neutral tail groups tend to aggregate due to the collective short-range interaction.^{25, 26, 50} The tail aggregation observed in the MD simulation represented as gatherings of white spheres is exhibited in Figure 3. Lopes and Pa'dua also carried out computer simulation using an all-atom force field on the 1-alkyl-3-methylimidazolium family with hexafluorophosphate (PF_6^-) or with bis(trifluoromethanesulfonyl)amide (TFSI) as the anions and obtained a similar results as that of Wang *et al.*⁴⁹ For ILs with alkyl chain length of $n \geq 4$, the aggregation was observed and the nonpolar domains permeated a three-dimensional network of ionic channels formed by anions and by the imidazolium rings of the cations. As the length of the alkyl chain increased, the nonpolar domains became larger and more connected and caused swelling of the ionic network.

Nanoscale segregation of small ILs with short alkyl chains ($n = 2, 3$), such as ethylammonium and propylammonium ILs, were also reported by small-angle neutron scattering.²³ In this case, solvophobic interaction between alkyl groups was also considered to be the most important factor for the

occurrence of heterogeneity, but the electrostatic and hydrogen bonding attractions between cations and anions were also considered important.⁵¹ Experiments^{52, 53} and computer simulations^{54, 55} suggest that a hydrogen bond network is formed between the acidic hydrogen on the aromatic ring of cation and the halogen anion or fluorine atoms of anion which also contributes to the self-organized heterogeneity of IL.

2.2. Interaction of ILs with other materials and molecules

Interaction of ILs with other molecules and materials can also lead to formation of unique heterogeneous structures. It is well known that nanoparticles^{56, 57} and nanostructures, such as nanowires,⁵⁸ gold dendrites,⁵⁹ nanoflowers,⁶⁰ and microporous lamellar silica,⁶¹ can be formed and stabilized in ILs. The heterogeneous structure of ILs induced by solvophobic interaction of alkyl chains and hydrogen bond network are considered responsible for the fabrication of well-defined extended ordering of nanoscale structures.⁶² Ueno *et al.* reported that when polymer grafted silica particles (silica core radius: ca. 60 nm) were suspended in ILs, a soft glassy colloidal array was formed and exhibited homogeneous, non-brilliant, angle-independent structural colors.^{63, 64}

Mezger *et al.* reported layering of ILs on charged surface by high-energy x-ray reflectivity study.⁶⁵ Three types of ILs with tris(pentafluoroethyl)trifluorophosphate anion on a charged sapphire substrate showed strong interfacial layering with spacing of ca. 8 Å, starting with a cation layer at the substrate and decaying exponentially into the bulk liquid. Figure 4 shows the cation, anion, and total electron density profiles at the IL-sapphire interface obtained from the best fit at temperature of -15°C . d_0 is the distance between the substrate's surface and the center of the first ion layer, while d is the layer spacing (ca. 8 Å). Inset shows a layering arrangement of correlated ions on a sapphire surface with double-layer stacking. These results strongly suggested that the observed molecular layering is a generic feature of ILs at charged walls. Atkin *et al.* also observed layered structure of ILs on solid surfaces by an atomic force microscope.^{66, 67} The measurements revealed oscillatory behavior with the size of the oscillations corresponding to the physical dimension of the ion pair. The greatest number of solvation layers was observed for ethylammonium nitrate on a highly charged atomically smooth mica substrate,

i.e., at least six layers with a width of 0.5 nm extending to a length of 3 nm.⁶⁶ Fewer and more compressible layers were observed for propylammonium nitrate due to the increased molecular flexibility. On a graphite substrate, two or three layers were detected and it was considered that the alkyl chains of cations was the source of the attractive interaction which was stronger for propylammonium nitrate due to the increased size of the alkyl moiety.

When other molecules are mixed or dissolved in a IL, the molecule may be located at a particular position in the heterogeneous liquid structure depending on its physical properties and it could also affect the nanostructure. Voth and coworkers have carried out MD simulation on imidazolium IL and water mixtures at various concentrations.⁶⁸ At low concentrations, water molecules were embedded in the network formed by anions and imidazolium head group of cations. The most ordered nanostructure of micelles (cation-cation) and water-anion networks were formed when the hydrogen bonding ability of the anions was saturated by water. At higher concentrations, the polar/nonpolar phase separation was well-diluted and ions became dispersed in the water clusters. In the case of acetonitrile (Acn),⁶⁹ MD simulation showed that Acn molecules are located in the interfacial regions between the ionic networks and the nonpolar domains with the negatively charged nitrogen atom pointing toward the positively charged head-group of the cation as shown in Figure 5. Acn molecules did not show aggregation with increasing concentration, which is consistent with the complete miscibility of Acn with ILs. In the case of aromatic hydrocarbons (benzene, toluene, and xylenes), clathrate formation was reported between 1-alkyl-3-methylimidazolium ILs.⁷⁰ Moreover, for 1,3-dimethylimidazolium hexafluorophosphate–benzene system, 2:1 inclusion compound was crystallized and the crystal structure showed that the benzene molecules are isolated within a staggered π – π ‘sandwich’ between two imidazolium cations. Neutron diffraction showed that the addition of benzene to the IL leads to an expansion of the cation-cation contacts, in agreement with the single-crystal structure.⁷¹ Benzene was also found to be homogeneously distributed throughout the IL with no evidence of micellar formation.

The molecular dynamics of solute can be also affected by its location within the microscopic liquid structure. Translational diffusion of emissive solutes in ILs was detected by fluorescence

correlation spectroscopy and it exhibited a bimodal behavior, indicating a presence of two distinct environments with different microscopic viscosity.⁷² Diffusive rotation of solute molecules in ILs was studied by anisotropy decay measurements⁷³⁻⁷⁸ and it is reported that the molecular dynamics are dependent on how the solute interacts with its surrounding.⁷⁶⁻⁷⁸ Fruchey and Fayer measured temperature-dependent fluorescence anisotropy decay of perylene and its derivative, sodium 8-methoxypyrene-1,3,6-sulfonate (MPTS), in a series of 1-alkyl-3-methylimidazolium ILs and the two fluorescent probe molecules displayed markedly different rotational dynamics when analyzed using Stokes-Einstein-Debye theory.⁷⁶ The orientational relaxation of perylene was faster than predicted by hydrodynamic theory and was ascribed to slip to subslip behavior. In addition, the rotational relaxation time showed increasingly subslip behavior as the length of alkyl chain was increased. These results indicated that perylene partitions into alkane-like environments. In contrast, MPTS showed superstick boundary behavior, likely reflecting very strong coordination with the RTIL cations, *i.e.*, three RTIL cations are bound to the three MPTS sulfonate anions, and the entire assembly undergoes orientational diffusion. The friction increased with increasing size of the solvent cation, which was consistent with the picture of cations bound to the MPTS sulfonate anion.

2.3. Red-edge effect

Spectroscopically, the distribution of solute molecules within heterogeneous liquid structure of ILs can be detected by the "red-edge effect" (REE) which has been often observed for fluorescent molecules doped in polymers and glasses.⁷⁹ Polymers and glasses can be considered as a medium with extremely slow relaxation dynamics, *i.e.*, full solvation takes infinitively long time. Accordingly, the absorption spectrum of the solute is affected by the inhomogeneity of the medium and when the solute is excited near the 0-0 transition or at longer wavelengths, the wavelength of the emission intensity maximum is dependent on excitation wavelength. In the case of highly viscous IL, fluorescent molecules with excited state lifetimes shorter than the solvation time is expected to exhibit REE.^{29, 80-84} Samanta and coworkers investigated this subject extensively,⁸⁰⁻⁸² and found excitation wavelength dependent shift of the

fluorescence maximum as large as 10-35 nm in some cases. REE for a fluorescent dye, 2-amino-7-nitrofluorene (ANF), the excited state lifetime of which is about 100 ps, in 1-butyl-3-methylimidazolium tetrafluoroborate (BmimBF_4) is shown in Figure 6. Hu and Margulis confirmed by MD simulation that the origin of the REE is the existence of persistent excited-state environments that do not reach the equilibrated solvation structure within the fluorescence lifetime, because of the slow translational and reorientational cage dynamics of IL.^{29, 85} For coumarin 153 (C153) with excited state lifetime of ca. 4.8-5.2 ns, REE was not very clear in an ammonium IL,⁸³ while it was significant (shift of 5-15 nm) in N-methylmorpholinium ILs which are considered to be more structured than other ILs.⁸⁶ Interestingly, the average solvation times of these ILs were 0.4-1.3 ns which are still shorter than the excited state lifetime of C153, indicating that the slower solvation process, which is the origin of REE, is not detected by this probe.

The heterogeneity of IL can provide different reaction fields for individual solute molecules. Kimura and coworkers have carried out investigation on excited state intramolecular proton transfer (ESIPT) reaction of 4'-N,N-diethylamino-3-hydroxyflavone (DEAHF) in IL.⁸⁷⁻⁸⁹ From the steady-state fluorescence spectra, it was found that the relative fluorescence intensity of the tautomer produced by ESIPT decreased by red-shifting the excitation wavelength from 380 to 450 nm.⁸⁷ From the time-resolved fluorescence spectra obtained by optical Kerr gate method, the early reaction process in several hundred picoseconds region was strongly dependent on the excitation wavelength.^{87, 89} Time-resolved fluorescence line shapes of DEAHF in 1-butyl-3-methylimidazolium hexafluorophosphate (BmimPF_6) obtained at 400 nm (bottom left) and 430 nm (bottom right) excitations are shown in Figure 7. According to the theoretical calculations,⁸⁸ the solvation coordinate of the Franck–Condon excited state is energetically unstable, although the tautomeric excited state is well solvated at this position of the solvent coordinate. Therefore, as solvation of the initial excited state progresses, the reaction barrier becomes high. As a consequence, the molecules excited at red-edge are more solvated than those excited at shorter wavelengths, leading to higher reaction barrier and lower yield of the tautomer as shown in the schematic illustration in Figure 7 (top).

3. Optical Kerr effect measurements in ILs

One of the most popular method to measure intermolecular dynamics of neat liquids and solids is femtosecond heterodyne detected optical Kerr effect (OKE)⁹⁰⁻⁹³ and it was also applied to ILs.⁹⁴ OKE response of IL is expected to be extended in wide range of time scales because of its heterogeneous structure, *i.e.*, ions inside local structure can rattle very rapidly while reorganization of larger scale liquid structure occurs in a longer time scale.²⁸ For pyrrolidinium ILs, Shirota *et al.* reported that the overdamped relaxation for time scales longer than 2 ps can be fitted by a triexponential function, with time constants of ca. 2 ps, 20 ps, and longer, and the slowest relaxation correlated with the viscosity in accordance with the Stokes-Einstein-Debye hydrodynamic model.⁹⁵ The intermolecular vibrational spectra obtained by Fourier transform of the OKE signal usually exhibits three or more modes in the range of $\leq 100 \text{ cm}^{-1}$. In the case of imidazolium ILs, Wynne and coworkers found three Brownian oscillator type modes with frequencies around 30, 65 and 100 cm^{-1} , and attributed them to the out-of-plane librations of the imidazolium ring with the frequency depending on the local configuration of anion.⁹⁶ They also observed an intense low frequency mode in the range of $< 1 \text{ cm}^{-1}$, in accordance with the existence of mesoscopic structure arising from aggregates or clusters that explains the anomalous and inconveniently high viscosities of ILs.⁹⁷ Quitevis and coworkers attributed the oscillation at 140 cm^{-1} , observed for 1-alkyl-3-methylimidazolium ILs with alkyl chain length of $n = 4-6$, to the corrective motion of locally ordered domains with steep intermolecular potentials that are unique to these ILs.⁹⁸

Quitevis and coworkers also investigated temperature dependence of OKE signals and reported that the intermolecular spectra of ILs with small inorganic anions are temperature independent, while those with bulky anions are dependent.⁹⁹ Because neutron diffraction measurement revealed presence of charge ordering in ILs with simple small anions,¹⁰⁰ they concluded that the temperature independence of the OKE spectra is due to the presence of "solid-like" domains in the ILs. Defects such as adjacent two ions of the same charge form gaps between the domains, and these gaps facilitate thermal expansion without affecting the structure of the domains. They also measured fraction dependent OKE dynamics of

binary mixture of imidazolium ILs with different types of anions and found out that the intermolecular spectrum of the mixture in the range of 0-250 cm^{-1} were well described by the weighted sum of the spectrum of each IL.¹⁰¹ The additivity of the OKE spectra were explained by a model in which ILs are not completely mixed but microscopically segregated into "block co-networks" of ILs constituted from same pairs of cation and anion. For binary mixtures of ILs with anions that differ greatly in size, such as Br^- and TFSI^- , presence of "block co-networks" were indicated, while those with anions that are nearly the same in size, such as PF_6^- and CF_3CO_2^- , get mixed quite randomly.¹⁰²

Shirota *et al.* reported reduction of shear viscosity by heavy atom substitution on both cations and anions of ILs.¹⁰³⁻¹⁰⁵ By changing neopentyl substitute to trimethylsilylmethyl substitute ($\text{C} \rightarrow \text{Si}$) for 1-methyl-3-alkylimidazolium cation, the shear viscosity was reduced by a factor of 1.6-7.4.¹⁰³ They also reported reduction of viscosity by anion in the order of $\text{PF}_6^- > \text{AsF}_6^- > \text{SbF}_6^-$.^{104, 105} Interestingly, OKE experiments showed that the substitution effect of cation from carbon to silicon was obvious in the high-frequency region (100-150 cm^{-1}) of the intermolecular modes where the rotational libration is dominant, while that of the anion affected the low-frequency region ($< 50 \text{ cm}^{-1}$) where the translational interaction-induced motion is dominant. MD simulation revealed that the interaction between cation and anion decreases with increasing ionic volume. They have found that phosphonium ILs also show lower shear viscosities and lower glass transition temperatures than their corresponding ammonium ILs.¹⁰⁶ The substitution of a (2-ethoxyethoxy)ethyl group for an octyl group in ammonium and phosphonium cations also reduced the shear viscosity and increased the surface tension.¹⁰⁶ Intermolecular spectra obtained by OKE measurements for these ILs indicated that the ether group in the cations gives stronger interionic interaction but with a more flexible and/or less segregated nature than the alkyl group. These results suggest the importance of investigating the relation between the heterogeneity in liquid structures and the interacting force between the ions.

4. Solvation in ionic liquid

For molecules undergoing charge separation or a large change of electric dipole moment in the excited state, the Stokes shift between the maxima of steady state absorption and fluorescence spectra depends on the polarity of solvent, which is explained by the Mataga-Lippert model of solvation.¹⁰⁷⁻¹¹⁰ The response of solvent against newly produced charge or dipole is important for ET and CT reactions and the dynamics of solvation has been studied extensively for normal solvents. In the case of IL, cations and anions can move individually in principle, which could lead to a difference in the structure and the dynamics of solvation compared to normal solvents. On these points, a number of investigations have been also reported in these years.

Note that OKE measurement monitors the decay of photoinduced polarizability anisotropy of a liquid, while solvation is an energy relaxation process of a solute induced by the motion of dipoles and charges of solvent. To directly elucidate the dynamical information about solvation, methods such as dynamic Stokes shift (DSS) and three-pulse photon echo peak shift (3PEPS) measurements are necessary.

4.1. Dynamic Stokes shift (DSS) measurement

Several review articles concerning solvation dynamics^{82, 94, 111-114} and related chemical reactions¹¹⁵ in ILs have been published. The most common experimental method to investigate the time evolution of solvation process is the DSS measurement, *i.e.* time dependent frequency shift of the fluorescence spectrum. In this method, dye molecules accompanying an increase of electric dipole moment upon photoexcitation are utilized as a probe. In polar solvents, such probe molecules exhibit a time-dependent red-shift of the fluorescence spectrum due to solvation dynamics as described schematically in Figure 8. In the case of normal polar solvents with static electric dipole, rotation of solvent molecules mainly contribute to the dynamics, while for IL, translation of ions is also considered to take an important role.

For the DSS measurements in IL, time-correlated single photon counting (TCSPC) technique with time resolution of typically ≥ 20 ps is often applied, of which measurement provides the information on the diffusive part of the solvation.^{74, 116-125} In order to monitor the ultrafast "inertial

response" of the solvent occurring in the time region much shorter than the time resolution of TCSPC, some suitable method are necessary such as fluorescence up-conversion^{126, 127} based on sum-frequency generation in an optical nonlinear crystal, or optical Kerr gate utilizing liquid or glass as a Kerr media for gating the emission.^{128, 129} Time resolution of the former technique can reach 45 fs,¹³⁰ although, in most cases, it is limited to 150-200 fs, and that of the latter is typically in the range of ≥ 200 fs due to the finite response of Kerr media. DSS measurement is sometimes time-consuming to cover the entire emission wavelength. Usually, fluorescence time profiles are measured at various wavelengths and the time-resolved fluorescence spectrum is reconstructed from these profiles by referencing the steady-state emission.^{30, 35, 37} The fluorescence intensity at each delay time is approximated by assuming that integrated intensity of the fluorescence profile at each wavelength is proportional to that of the steady-state fluorescence spectrum. After the reconstruction of the time-resolved spectrum, the peak frequency is extracted by fitting the spectrum with appropriate functions. Solvation correlation function is obtained from the time dependence of the peak frequency, which is defined as,

$$S(t) = \frac{\nu(t) - \nu(\infty)}{\nu(0) - \nu(\infty)}, \quad (1)$$

where $\nu(t)$ is the peak frequency at delay time t and the time constant for solvation process can be obtained by least-squares-fitting of $S(t)$.

Only a few investigations with subpicosecond time-resolution have been reported so far.^{111, 122, 125, 131, 132} Maroncelli and coworkers applied fluorescence upconversion and optical Kerr gate technique with time-resolution of ca. 80 fs and 450 fs, respectively, to the DSS measurement.^{111, 122, 125, 131} By combining it with TCSPC technique, they obtained the solvation response in ILs in wide time range. Figure 9 shows a typical examples of $S(t)$, which were obtained from DSS measurement of typical probe molecule, coumarin 153 (C153), in some of the typical imidazolium ILs. The response functions could be separated into a subpicosecond inertial component, which accounts for 10-40% of the response, and a much slower diffusive component. The time constant of the fast component had a correlation with the ion mass, while the slower diffusive component was correlated with the solvent viscosity.

In the time range of picoseconds and longer, solvent molecule collides with each other numerous times and the solvent motion becomes diffusive. Accordingly, bulk viscosity affects the solvation dynamics in the longer time scale. On the other hand, the number of collision decreases in the shorter time range and only a few collisions occur at extremely short times. In an ultrashort time scale, molecules can move freely without collision for a microscopic distance. In usual polar solvents, very small angle free rotation of a few solvent molecules in the vicinity of the solute has been considered to contribute to the primary process of solvation.¹³³ Such a motion is called "inertial" or "non-Markovian" process, which was first claimed to be observed for acetonitrile by Fleming and coworkers.^{39,40} For the case of IL, it is theoretically considered that individual or collective translational motion of ions in the vicinity of solute are responsible for the subpicosecond solvation.¹³⁴⁻¹³⁶ We will discuss the details of ultrafast inertial response in the following section.

The diffusive solvation of IL in the picosecond range or longer can be monitored by TCSPC technique and variety of studies have been reported.^{74, 114, 116-121, 123, 124, 137, 138} The process is strongly dependent on viscosity and the response function is often described by multi-exponential, $\sum_n A_n \exp(-t/\tau_n)$, or stretched exponential, $\exp[-(t/\tau)^\beta]$, functions with the value of β in the range of 0.4-0.6. These β values are close to those obtained for viscous supercooled liquids.^{139, 140} Maroncelli and coworkers concluded that simple dielectric continuum model, which have been providing remarkably accurate predictions of solvation dynamics in conventional dipolar solvents,^{35, 141-143} systematically underestimated the solvation times by factors of 3-5.¹¹¹ It was suggested that one reason for this shortcoming was related to the spatial dispersion in the polarization response of ILs which was not taken into account in the simple dielectric continuum model.

In the scope of linear response theory, solvation dynamics should not depend on the amount of dipolar difference before and after the photoexcitation, *i.e.* $S(t)$ is independent of the reorganization energy. Theoretically, it is reported that this is also the case for ILs, *i.e.* no significant probe dependence has been observed for solvation energy relaxation although the magnitude of DSS varies with the dipole

moment of the excited solute.¹⁴⁴ Accordingly, solvation dynamics should not depend on the position of the initial population generated on the excited state potential surface in homogeneous solvent which could be approximated as a dielectric continuum. However, in the case of heterogeneous medium which is microscopically segregated into high and low viscosity areas, $S(t)$ can depend on the location of the solute molecule. In the case of coumarin 480 (C480) in a dimyristoyl-phosphatidylcholine vesicle, the solvation time was found to be 1.5 ps for excitation at 430 nm, while at 390 nm, two substantially slower components of 250 and 2000 ps were found.¹⁴⁵ It is considered that excitation at 430 nm preferentially selects the probe molecules in the water pool of the lipid, while for the 390 nm excitation, C480 molecules in the hydrophobic and restricted locations inside the lipid bilayer is probed.

Jin *et al.* investigated wavelength dependence for C153 in dimethyl-isopropyl-propyl-ammonium TFSI by means of TCSPC method with instrument response of 25 ps and reported that, while rotational diffusion was found to be homogeneous, the solvation time was heterogeneous.⁸³ Most of their excitation wavelengths were, however, not on the red-edge of the absorption band but rather close to the absorption maximum or even at shorter wavelengths. When the excitation wavelength is over-tuned to shorter wavelengths, the molecule is excited to higher vibrational levels of the excited state and intramolecular relaxation would also blend into the dynamics which is the reason why REE is observable only at the red-edge of the absorption spectrum. Further investigation is necessary concerning this subject.

4.2. Three-pulse photon echo peak shift measurement

Nonlinear coherent spectroscopy with ultrashort time resolution, such as three-pulse photon echo peak shift (3PEPS) technique, has also been applied to measure solvation dynamics.^{34, 36, 146-149} Generically, the time-resolution of this method is solely limited by the pulse duration and it is also applicable to weakly polar systems with very small Stokes shift.¹⁵⁰ 3PEPS was first applied to room temperature solutions by Joo and Albrecht¹⁵¹ and then it was theoretically proven to be related to $S(t)$.¹³³

Photon echo is a time domain analogue of the hole-burning spectroscopy. Two sequential pump pulses create a hole in the absorption spectrum with the shape of the hole being the Fourier transformed spectrum of the two pulses with a delay. The echo signal is the diffraction of the third probe pulse by the interference pattern generated by the two pump pulses and it is delayed from the third pulse due to the reverse-Fourier transform of the hole-spectrum. The coherent polarization created in the sample by the first pulse needs to be maintained until the arrival of the second pulse in order to create an interference pattern, while thermal fluctuation induces decoherence and reduction of the echo signal. Even if the interference pattern is created, the echo signal will be reduced if the hole-spectrum is disturbed by the thermal fluctuation before the arrival of the third pulse. If the entire phase information is eliminated by the fluctuation, the signal becomes equivalent to that of transient grating which is generated simultaneously with the arrival of the third pulse. Accordingly, echo peak shift provides information on the time scale of molecular fluctuation in condensed phase.

For 3PEPS measurement, the intensity of the diffracted beam is measured as a function of the time interval between the first and the second pulses, t_{12} , while keeping the one between the second and the third pulses, t_{23} , at a certain value. Two echo signals diffracted at phase-matching directions of $-\mathbf{k}_1 + \mathbf{k}_2 + \mathbf{k}_3$ and $\mathbf{k}_1 - \mathbf{k}_2 + \mathbf{k}_3$ are simultaneously measured. The shift of the echo intensity maximum from the zero delay, $t_{12} = 0$ fs is referred to as the peak shift, $\tau^*(t_{23})$, which is accurately obtained as a half of the time interval between the maximum of the two signals, whose value is obtained by least-squares fitting with Gaussian function. The plot of $\tau^*(t_{23})$ vs. t_{23} constitutes the 3PEPS data set. According to the fluctuation dissipation theorem, at high temperature limit, $S(t)$ is equivalent to the solvent fluctuation correlation function, $M(t)$,¹⁵²

$$M(t) = \frac{\langle \delta\omega_{eg}(0)\delta\omega_{eg}(t) \rangle}{\langle \delta\omega_{eg}^2 \rangle} \quad (2)$$

where $\delta\omega_{eg}$ represents the amount of fluctuation of the transition frequency. Approximately, 3PEPS data, $\tau^*(t)$, is related to $M(t)$ by the equation,¹³³

$$\tau^*(t) = \frac{M(t)}{\sqrt{\pi[\langle \Delta^2 \rangle + \lambda^2 f(t)]}} \quad (3)$$

where $\langle \Delta^2 \rangle$ is the coupling strength, λ is the reorganization energy, and $f(t) = [1 - M(t)]^2$. Therefore, solvation dynamics can be monitored by 3PEPS measurement.

3PEPS measurement has been applied not only to simple solvents but also to polymers¹⁵³⁻¹⁵⁵ and biological systems.¹⁵⁶⁻¹⁶¹ The first application to IL was performed by Lang *et al.*¹³² and reported a time profile up to delay of 600 fs although their experiment was not conclusive. We also investigated the ultrafast solvation process of imidazolium ILs in the range of ≤ 100 ps by means of 3PEPS experiment with time-resolution as high as 30 fs.¹⁶² An organic dye, oxazine 4 (Ox4), was used as a probe molecule, because this dye has been frequently employed in photon echo experiments in various environments¹⁶³⁻¹⁶⁶ and the comparison of the results with the previous articles could provide detailed information on the peculiarity of ILs. Moreover, as a cationic dye, Ox4 is expected to be located in the polar region of the heterogeneous IL and to be sensitive to the motion of anions.

3PEPS signal obtained in ILs are shown in Figure 10, where the result in ethanol (EtOH) is also exhibited for comparison. The 3PEPS signals of all solutions exhibit oscillatory modulation in the time range of ≤ 10 ps, due to the coherent intramolecular vibrations of Ox4. In the range of ≥ 10 ps, the 3PEPS in EtOH decays more significantly than those in ILs because of the lower viscosity (1.1 cP at 298 K). The solvation process in EtOH is nearly accomplished within ≤ 100 ps, while those in ILs extend into the range of > 100 ps due to their high viscosity (> 30 cP). Ultrafast part of the $M(t)$ obtained for ILs are shown in Figure 11, where signals with intramolecular vibrations and asymptotic component were excluded. The decay shows no remarkable dependence on the alkyl chain length of the cation in the time range of ≤ 200 fs (Figure 11b), while a correlation with the size of anion is suggested (Figure 11a), i.e. smaller and lighter anion exhibits faster decay. For Bmim⁺, the time constant for the fastest decay component increases in the order of Cl⁻ (26 fs) < BF₄⁻ (110 fs) < PF₆⁻ (150 fs) < TFSI (210 fs).

From the DSS measurements, Maroncelli and coworkers concluded that the initial ultrafast decay is related to inertial ion motions, because it had a correlation with the factor, $\sqrt{\mu_{\pm}(R_{+} + R_{-})^3}$, where μ_{\pm} is the reduced mass of an ion pair and $(R_{+}+R_{-})$ is the sum of their van der Waals radii.¹²² In our case, the time constant had a better correlation simply with the square root of anion mass, $m_{-}^{1/2}$, as can be seen in Figure 12a. Because Ox4 is a cationic dye, it may be located in the microscopic polar domain of the IL and have a stronger interaction with the anion of IL. Molecular dynamics computer simulation suggests that subpicosecond inertial regime of solvation is mainly governed by the motions of a few adjacent ions in the case of a dipolar solute with sufficiently high density of surrounding ions.^{134, 135} Especially, the motion of Cl⁻ in the first solvation shell dominates the ultrafast regime due to its small size which enables closer location to the solute. Interestingly, the second time constant had a slightly better correlation with $\sqrt{\mu_{\pm}(R_{+} + R_{-})^3}$ rather than $m_{-}^{1/2}$ (Figure 12b), suggesting the beginning of more global solvation process including the motion of cations. Similar trend has been also reported by optical Kerr effect measurement of 1-heptyl-3-methylimidazolium ILs, the time constant for the nondiffusive part of the orientational response increased in the order of Br⁻ (117 fs) < PF₆⁻ (215 fs) < TFSI⁻ (354 fs).⁴⁴

Interestingly, Maroncelli and coworkers reported that the ammonium and phosphonium ILs lack the ultrafast portion of the response,¹³⁷ while we observed sub-hundred femtosecond solvation response in phosphonium IL. Because Ox1 is an organic salt and more polar than their fluorescent probe, C153, this could be the manifestation of the heterogeneity of IL or it could be due to the methodological difference. Daschakraborty and Biswas considered a Lennard-Jones interaction for the nearest neighbor solute-solvent nondipolar interaction and concluded that 3PEPS and DSS experiments may be sensitive to different components of the total solvation dynamics.¹⁶⁷ Because 3PEPS measurements is related to the line-broadening function which is determined by the total solvation energy correlation function,^{168, 169} both polar and non-polar solute-solvent interactions contribute to the peak shift.¹³³ Thus, the ultrafast solvation response of ILs measured by 3PEPS experiments may have an origin in the nearest neighbor solute-solvent non-dipolar interaction. Kashyap and Biswas suggested that absence of the ultrafast

component of DSS in ammonium and phosphonium ILs is because none of the ions constituting these ILs possesses permanent dipole moment.¹⁷⁰

5. Electron transfer reaction

In this section, we will briefly go through the theoretical model developed for ET and discuss their application to experimentally observed ET in ILs. Because of the heterogeneity and wide range of dynamical time-scale, simple model based on transition state theory may not be applicable to ET in ILs.

5.1. Models of electron transfer

According to the general Marcus theory of ET, the electronic coupling factor, V_{el} , between reactant and product state is the major rate limiting factor in the nonadiabatic limit and the rate constant for ET can be expressed as;^{171, 172}

$$k_{NA} = \frac{2\pi}{\hbar} \frac{V_{el}^2}{\sqrt{4\pi\lambda_s k_B T}} \exp\left(-\frac{\Delta G^*}{k_B T}\right) \quad (4)$$

where k_B , T , ΔG^* , and λ_s are the Boltzmann constant, absolute temperature, activation energy, and solvent reorganization energy, respectively. As can be seen from Equation 4, when $\Delta G^* = 0$, the rate constant is determined by V_{el} . Meanwhile, at the adiabatic limit where the coupling between the two state is significantly strong, not V_{el} but the solvation time, τ_s , that represents the time scale of solvation dynamics, becomes the rate limiting factor;³¹

$$k_A = \frac{1}{\tau_s} \sqrt{\frac{\lambda_s}{16\pi k_B T}} \exp\left(-\frac{\Delta G^*}{k_B T}\right). \quad (5)$$

In this expression, solvation dynamics sets an upper limit to the rate of ET in the adiabatic regime.

However, not only solvent reorganization but also intramolecular nuclear reorganization can also contribute to ET. In such a case, the reaction takes place through couplings between the discrete vibrational levels of reactant and product states and the rate constant becomes the summation of each rate constant between vibrational levels of reactant and product states with vibrational quantum number

of v_r and v_p , respectively, multiplied by the population ratio of the reactant in the vibrational level v_r , $p(v_r)$,^{173, 174}

$$k_{NA} = \sum_{v_r, v_p} k_{NA}(v_r, v_p) p(v_r), \quad (6)$$

with

$$k_{NA}(v_r, v_p) = \frac{2\pi}{\hbar} \frac{V_{el}^2}{\sqrt{4\pi\lambda_s k_B T}} \exp\left(-\frac{\Delta G'_0 + \lambda_s}{4\lambda_s k_B T}\right), \quad (7)$$

where $V_{el}^2 = FC(v_r, v_p)V_{el}^2$ with $FC(v_r, v_p)$ being the Franck-Condon factor between the vibrational level v_r and v_p and $\Delta G'_0 = \Delta G_0 + \Delta\varepsilon(v_r, v_p)$ with ΔG_0 and $\Delta\varepsilon(v_r, v_p)$ being activation energy for the lowest vibrational level and the vibrational energy difference between level v_r and v_p , respectively. Especially in the Marcus inverted region, multiple crossing points to the higher vibrational levels of the product state induces faster ET compared to the case without the vibrational contribution.

Although these theoretical treatments have been contributing to the elucidation of ET and related processes, these models are in the regime of transition state theory which assumes thermal quasi-equilibrium that the relative ratio of the reactant molecule in the transition state is constant during the course of a reaction. In the case that the driving dynamics of the reaction is biphasic with fast and slow diffusions, however, the reactant molecules near the transition state could diminish faster than the ones located further away, because the slow diffusion cannot catch up with the reaction. In such a case, diffusion of molecules on the reaction coordinate needs to be described numerically and such a model was first developed by Bagchi, Fleming, and Oxtoby for the ultrafast nonradiative decay of excited state, *i.e.* molecules diffuse on the excited state potential energy surface and the decay occurs through a position-dependent “sink” with a certain functional form such as Gaussian or Lorentzian.¹⁷⁵ Sumi, and Marcus further developed a model with two-dimensional coordinate that describes fast and slow diffusions.⁴¹⁻⁴³ Diffusion is considered to be very fast along one coordinate where the quasi-equilibrium is always maintained, while it is slow on the other where the population distribution evolves with time.

It is assumed that transition state theory holds along the fast coordinate with rate constant, $k(X)$ that depends on the position on the slow coordinate, X ,

$$k(X) = \nu_q \exp\left[-\frac{\Delta G^*(X)}{k_B T}\right], \quad (8)$$

where $\Delta G^*(X)$ is the activation energy at point X and ν_q is the pre-exponential factor. Meanwhile, diffusion along the slow coordinate, X , is treated by a diffusion-reaction equation,

$$\frac{\partial p(X, t)}{\partial t} = D \frac{\partial}{\partial X} \left[\frac{\partial}{\partial X} + \frac{1}{k_B T} \frac{dV(X)}{dX} \right] p(X, t) - k(X)p(X, t), \quad (9)$$

where $p(X, t)$ is the reactant distribution at point X at time t , D is the diffusion coefficient, and $V(X)$ is the energy surface along the coordinate X . The first term on the right-hand side represents the diffusion along the coordinate X and the last term represents the reaction occurring at each X . Usually, multiple degrees of freedom exist for motion of a molecular system in condensed phase which could be either fast or slow. For polymers and proteins, the large motion of the main chain could be slow while localized motion of individual sites and branches could be fast. Even for a simple molecule, intra- and inter-molecular dynamics can occur in different time scales. ET faster than diffusive solvation dynamics have been actually observed in conventional polar solvents.^{31, 176-180} These theoretical treatments and experimental results suggest that ultrafast ET process could occur also in highly viscous and heterogeneous ILs.

In the two dimensional model, the reaction rate is dispersed and the reaction becomes multiexponential due to the activation energy which depends on the position of the slow coordinate, X , as can be seen in Equation 8. This situation is similar to the excitation wavelength dependence of ESIPT for DEAHF as discussed in the earlier section, *i.e.*, the activation energy for ESIPT depends on the degree of solvation.⁸⁷⁻⁸⁹ Also for a diphenylmethane dye, auramine O, the rate of nonradiative decay of the excited state were found to be much more dispersed in IL compared to those in normal solvents.^{181, 182} It is known for auramine O that the twisting motion of phenyl rings promotes the nonradiative decay which is dependent on solvent viscosity. Thus, the high viscosity of IL hinders the twisting motion and,

not the heterogeneity of IL, but the distribution of the twisting angle was considered to be the origin of dispersed decay rate for auramine O.

5.2. *ET and CT reactions in IL*

Several articles concerning the relation between ET reactions and solvation dynamics in IL have been published, although, the number of reports is still limited and systematic research is still under development.

Shim and Kim applied molecular dynamics computer simulation for ET processes of a model diatomic solute in IL and in acetonitrile and found that, even though overall solvent relaxation dynamics in IL were considerably slower than those in acetonitrile, the deviation of the rate constant from the transition state theory predictions is found to be small for both solvents.^{183, 184} This result was attributed to the viscosity dependent slow component of the solvent relaxation being of little importance in activation and deactivation of ET. It is indicated that the actual rate constant in ILs could be much higher than the extrapolation based on total viscosity. This situation, however, seems to be applicable only to the case where the activation barrier is rather high and consequently the influence of solvent dynamics is modest. As the barrier decreases, ET could be more strongly affected by the slower dynamics.

Experimentally, intramolecular photoinduced charge separation and recombination of 4-(N-pyrrolidino)naphthalene-1,8-imide-pyromellitimide (5ANI-PI) in EmimTFSI were studied by Lockard and Wasielewski.¹⁸⁵ They reported that the rate constants of both process were comparable to those observed in pyridine, which has a viscosity of nearly 2 orders of magnitude lower than that of the IL and suggested that both processes were more strongly influenced by the fast translational processes in IL rather than the slower motions that are related to bulk viscosity. On the other hand, Castner Jr. and coworkers investigated photoinduced ET processes of a donor–bridge–acceptor system, comprising a 1-N,1-N-dimethyl-1,4-phenylenediamine donor connected to coumarin 343 acceptor. They reported that photoinduced ET kinetics had broadly distributed rates that are generally slower in ILs compared to

conventional solvents where the rate of ET had narrower distributions.¹⁸⁶ In ILs, the time scales of solvation dynamics for the solute in the excited state overlap with that of ET and such entanglement of dynamics was considered to be the cause of broadly distributed reaction rates in IL. Meanwhile, Samanta and coworkers investigated intramolecular ET reaction of crystal violet lactone (CVL) in several ILs and found that this ET reaction is governed by the slow solvation dynamics, which is related to the viscosity.¹⁸⁷ As a consequence, the intramolecular ET of CVL was difficult to occur in highly viscous ILs with long solvation times. Samanta and coworkers also investigated the photoinduced CT of 4-(N,N'-dimethylamino)benzonitrile (DMABN) in ILs.¹⁸⁷ They found that the picosecond time-resolved emission spectrum exhibited decay of the LE state emission intensity and shift of the peak position of CT state emission with increasing time after the excitation. By analyzing the evolution of the CT state from the LE state and solvent relaxation of the CT state, They concluded that the LE→CT interconversion rate is determined not by the slow dynamics of solvation but the rate of structural reorganization of the molecule, namely, twisting around the bond between the dimethylamino and cyanophenyl moieties, which depends on the viscosity.

Several groups have studied intermolecular ET in IL by utilizing N,N-dimethylaniline (DMA) as a electron donor.¹⁸⁸⁻¹⁹⁰ Paul and Samanta studied ET reaction between pyrene and DMA in imidazolium ILs and found that exciplex emission is unobservable indicating high polarity of the IL.¹⁸⁸ The rate constant was 2-4 fold higher than the diffusion-controlled value suggesting that the microviscosity around the donor and acceptor is different from the bulk viscosity of the ILs. On the other hand, solvent-separated radical ions were unobservable in high-viscosity ILs because of a significantly lower escape rate compared to the geminate recombination. Bhattacharyya and coworkers observed Marcus-inverted region for the ET of coumarin/DMA system in IL.¹⁸⁹ In the absence of DMA, a rise component was observed in the time-dependence of emission at longer wavelengths due to the DSS. On the contrary, no rise was observed in the presence of DMA (1.5 M) which indicates that ET is faster than the solvation. In neat DMA, similar effect has been known, *i.e.*, coumarin dyes exhibit blue shifted fluorescence due to ET faster than solvation.¹⁷⁶ It was concluded that, because of the very slow diffusion in IL due to the

very high viscosity and nanostructural organization of IL with polar and nonpolar domains, the donor and acceptor species could remain in close proximity, resulting in ET faster than solvation dynamics. ET reaction between 9,10-dicyanoanthracene and DMA in ILs was also studied by Maroncelli and coworkers.¹⁹⁰ It showed effective quenching rate constants which were often 10-100 fold larger than simple predictions for diffusion-limited rate constants. They concluded that the primary factor for such a large quenching rate was the high viscosities typical of ILs emphasizing the transient portions of reaction, *i.e.*, the reaction occurs in a multi-exponential manner with a time dependent rate constant, $k(t)$, which is always $k(t) > k(\infty)$. The second important factor was considered to be the Stokes-Einstein relationship significantly underestimating the diffusion coefficients in ILs because of the large size of IL constituents, especially the bulky cation with long alkyl chains. It was concluded that the diffusion coefficients in ILs exceeds hydrodynamic predictions by significant factors of 3-10.

9,9'-Bianthryl (BA), with a symmetric structure of two anthracenes connected in the middle as shown in Figure 1, is one of the typical examples that undergoes charge separation process in the excited state.^{107, 191-196} In nonpolar solvents, the excited state of BA localizes in either of the two anthryl moieties (LE state), while the charge separation between the two moieties takes place in polar solvents (CT state). This can be observed as a red shift of the fluorescence with increasing solvent polarity, *i.e.*, the spectrum in *n*-hexane peaks at ca. 413 nm with vibronic structures, while that in acetonitrile is a featureless broad band at ca. 465 nm. BA in IL exhibits a broad emission centered at ca. 472 nm, which is safely ascribable to the CT state.

The LE to CT conversion process of BA has been widely investigated in normal solvents by various ultrafast spectroscopic methods, of which investigations revealed that solvent fluctuation leads to the symmetry-breaking of the environment in the two moieties that triggers the CT process.^{107, 191-196} Photoinduced charge separation process of BA in Bmim⁺ ILs with three different types of anions was studied by means of transient absorption spectroscopy.^{197, 198} One of the results in the femtosecond to nanosecond time range is shown in Figure 13 and 14, respectively.¹⁹⁷ In the early stage after the excitation, transient spectra show an absorption maximum at ca. 580 nm which can be ascribed to the

LE state because the absorption maximum and spectral band shape are respectively similar to those observed in *n*-hexane solution.¹⁹⁶ Within a few hundred picoseconds, the absorption band at ca. 580 nm gradually decreases and a new band rises at ca. 690 nm, which can be assigned to the CT state.¹⁹⁶ In the nanosecond domain shown in Figure 14, except for the rise of the triplet state at 427 nm,¹⁹⁹⁻²⁰¹ the spectral band shape in the wavelength region of >550 nm showed no remarkable evolution.

Time profile of the transient absorption at 690 nm shows multiexponential rise of the CT state indicating contribution of multiple degrees of freedom to the intramolecular CT, the dynamics of which are distributed in wide range of time scales with the ones in the range of <20 ps being the major component. In the case of BmimTFSI, the rise can be fitted by triple exponential functions with time constants of ca. 450 fs (27 %), 7.5 ps (37 %), and 140 ps (36 %) with average of 53 ps. The average solvation time of BmimTFSI is reported to be in the order of 380-560 ps which is significantly longer than the value obtained from CT of BA.⁸² The shortest time constant is closer to the time range of the inertial response of BmimTFSI which is 310 fs (integral time). On the other hand, as can be seen from the emission spectrum shown in Figure 15, the shift of the CT state fluorescence of BA extends into longer time scale as comparable to that of the diffusive solvation.¹⁹⁸ Note that the weak shoulder at 24,000 cm⁻¹ corresponds to the residual LE state emission and its peak frequency is constant while its intensity decreases with time. These results indicates that LE to CT state interconversion takes place through fast fluctuations and rapidly reaches thermal quasi-equilibrium. Subsequently, level lowering of the CT state is induced by the slower diffusive solvation and the LE state is further depopulated. The situation is similar to that predicted by the 2D reaction model of Sumi and Marcus⁴¹⁻⁴³ discussed in the previous section.

Maroncelli and coworkers have also studied three excited-state intramolecular ET reactions of 9-(4-biphenyl)-10-methylacridinium (BPac⁺), CVL, and BA by time-correlated single-photon counting (TCSPC) technique.²⁰² In the case of BPac⁺ with sufficiently long lifetime (1-3 ns), isoemissive point was observed in the time-resolved fluorescence spectra indicating a simple two-state kinetics and the CT reaction times were strongly correlated to the solvation times in both IL and dipolar solvents. In the case

of the CVL reaction which is also nearly a two-state process, an approximate equality was found between CT reaction and solvation times. Finally, for the BA reaction, isoemissive point was undetected and the emission dynamics was more similar to that of a nonreactive probe undergoing solvation as reported previously. They also examined the time-dependence of the integrated intensity of the undifferentiated LE + CT emission band, as done previously by Barbara and co-workers for the dynamics in normal polar solvents,^{192, 203, 204} and concluded that the decay times associated with the integrated intensity are approximately equal to the solvation times in ILs.

It is worth noting that the relative fluorescence quantum yields and lifetimes of BA are reported to be almost unity and 8 ns in *n*-hexane and 0.41 and 35 ns in acetonitrile, respectively.²⁰⁵ Accordingly, the radiative rate constant of the LE state emission is ten times larger than that of the CT state. This difference in the radiative rate constants is reflected in the relative intensity of the LE and CT emission bands. In addition, initial emission being missed by the limited time-resolution of TCSPC may also contribute to the rapid CT process. Although preliminary fluorescence upconversion experiments with subpicosecond time resolution was reported,²⁰² the observation was only limited to the blue edge of the emission and the rapid CT process that was confirmed by transient absorption spectroscopy was not clearly elucidated. For BA in ethanol and butanol, a structured anthracene-type fluorescence spectrum is reported to transform into an unstructured emission spectrum in the subpicosecond domain.²⁰⁶ It is also reported that, in imidazolium ILs, time-resolved fluorescence spectrum of BA near the time origin exhibits a sharp peak at 420 nm which corresponds to that of the structured anthracene-type LE emission.²⁰⁷ Moreover, typical theoretical model assumes instantaneous formation of electric dipole moment by crossing the transition state. However, in the case of BA with strong coupling between the two states, the dipole moment produced by the CT reaction may continuously increase with the advance of solvation, accompanying the reduction of emission intensity.

Interestingly, Maroncelli and coworkers have compared "integral Stokes shift times" measured with BA and C153 and observed that the BA shifts were slightly slower than those of C153 in all cases.²⁰² However, the differences were within the anticipated uncertainties of the data in most cases,

and they concluded that the Stokes shift dynamics of BA reflected the slower portions of the solvation response. However, concerning the heterogeneity of IL, because BA is a symmetric molecule without any electric dipole in the ground state, solvation and CT dynamics of BA may differ from those of more polar solutes. Muramatsu *et al.* compared DSS of BA in several ILs with those of polar 4-(9-anthryl)-N,N'-dimethylaniline and C153 with ground state dipoles of ca. 5.0 and 6.6 Debye, respectively.²⁰⁸ In most of the ILs they have studied, $S(t)$ of both molecules were nearly identical with exception in trihexyltetradecylphosphonium (Phos) TFSI, *i.e.* the decay of $S(t)$ for BA was clearly slower than those of the others. This observation could be due to the peculiar initial microscopic solvent environment of the nonpolar BA. The $S(t)$ of phosphonium IL is reported to lack the ultrafast inertial subpicosecond component.¹³⁷ The difference in initial solvation structure will be erased by the ultrafast component for most of the ILs, while in PhosTFSI, this difference is preserved for longer times.

To elucidate the relation between the solvation time and ET/CT rate, we also investigated photoinduced CT processes of linear phenyleneethynylene derivatives (PEN) with different sequences of electron-withdrawing perfluorophenyl groups (A) and electron-donating phenyl groups (D) in BmimTFSI.²⁰⁹ The advantage of these systems is that polarity of the molecule can be changed systematically such as, AADD, ADDA, DAAD, or ADAD. For the polar molecule, AADD, very rapid photoinduced charge separation occurred which was neither detectable with our picosecond TA nor TCSP measurement setup with time resolution of 15-30 ps. Time-resolved fluorescence spectra exhibited time-dependent red-shift similar to that of BA as shown in Figure 16a, which indicates subsequent stabilization by the solvation of the CT state that was produced very rapidly. The time profile of the DSS for AADD in Figure 16b was similar to that previously obtained by C153 in BmimTFSI.^{117, 123} Interestingly, while total DSS of ca. 2500 cm^{-1} was observed, no time-dependent change of the spectral width was observed as shown in Figure 16b, where the time-resolved fluorescence spectra from 30 ps to 2.0 ns are shifted in frequency and almost complete overlap can be seen (similar overlap was also observed for the spectra of BA^{197, 198}). This indicates that the dynamics regulating the spectral broadening due to the CT reaction could be different than that inducing the spectral shift. The

fluorescence from the LE state was not detectable for AADD, although that of BA was detected as a weak shoulder on the blue side of the strong CT state emission. This difference might be partly due to the large radiative constant of the LE state of BA, while the radiative rate constant of the LE state of AADD observed in nonpolar solution was comparable with that of the CT state. In addition, the polar nature of AADD should be also taken into account. BA is a symmetric nonpolar molecule in the ground state, while AADD is polarized even in the ground state. This difference, may induce presolvation before the excitation, and as a consequence, it could induce rapid CT.

For weakly polar ADAD and ADDA, CT reaction was unobservable. The TA spectra of ADAD and ADDA exhibited absorption maxima at ca. 680 nm which can be attributed to the LE state, while that of AADD peaked at 725 nm which is the CT state. Interestingly, in the TA spectrum of quadrupolar DAAD, double maxima at 680 nm and 725 nm were observed indicating an establishment of equilibrium between the LE and CT states. Time-resolved fluorescence spectrum of DAAD also exhibited reduction of the peak at ca. 385 nm with appearance of a new band around 415 nm, indicating production and stabilization of the CT state as shown in Figure 17.

6. Concluding remarks

Room temperature IL possesses peculiar properties and it is anticipated to be a new type of solvent. Its heterogeneous liquid structure has been predicted by MD simulations and confirmed by X-ray diffraction experiments. The microscopic segregation of IL into nonpolar and polar domains contributes to formation and stabilization of various nanoparticles and nanostructures. As discussed in Section 2. 2, IL is known to form organized layers on a charged surface. Thus, IL is also expected to form specific structures around nanoparticles and solute molecules. The heterogeneity of IL as an solvent can provide a new type of reaction field. Dynamical aspects of solvation and chemical reactions in ILs have been investigated, although the number of studies are still limited. Time-resolved spectroscopies reveal the hierarchic nature of the solvation dynamics in IL which is similar to those in highly viscous liquids such as those in the super-cooled temperature regime. However, they do not provide information about

structural evolution of the solvation shell during the course of ET/CT reaction. At the present state, only the rate of ET and that of solvation have been compared and the effect of heterogeneous solvation on chemical reaction is yet to be explored. The initial location of the solute in the heterogeneous liquid structure depends on the polarity and other physical properties of the solute that interacts with the surrounding and we think that it could strongly affect the chemical reaction. As a future perspective, the coming research requires to detect the microscopic environment surrounding a solute and to directly monitor its time evolution during the course of a chemical reaction.

Acknowledgement

YN was supported by Precursory Research for Embryonic Science and Technology (PRESTO), Japan Science and Technology Agency (JST). HM was supported by a Grant-in-Aid for Scientific Research (23245004) from the Ministry of Education, Culture, Sports, Science and Technology (MEXT), Japan.

Reference

1. D. R. MacFarlane, M. Forsyth, P. C. Howlett, J. M. Pringle, J. Sun, G. Annat, W. Neil and E. I. Izgorodina, *Acc. Chem. Res.*, 2007, 40, 1165-1173.
2. P. Wasserscheid and W. Keim, *Angew. Chem. Int. Ed.*, 2000, 39, 3772-3789.
3. P. Wasserscheid and T. Welton, eds., *Ionic Liquids in Synthesis*, Wiley-VCH, Weinheim, 2003.
4. T. Welton, *Chem. Rev.*, 1999, 99, 2071-2083.
5. M. Armand, F. Endres, D. R. Mac Farlane, H. Ohno and B. Scrosati, *Nature Materials*, 2009, 8, 621-629.
6. J. P. Hallett and T. Welton, *Chem. Rev.*, 2011, 111, 3508-3576.
7. J. H. Davis Jr., *Chem. Lett.*, 2004, 33, 1072-1077.
8. J. Dupont, R. F. de Souza and P. A. Z. Suarez, *Chem. Rev.*, 2002, 102, 3667-3692.
9. M. J. Earle and K. R. Seddon, *Pure Appl. Chem.*, 2000, 72, 1391-1398.
10. M. Galinski, A. Lewandowski and I. Stepniak, *Electrochim. Acta*, 2006, 51, 5567-5580.
11. C. M. Gordon, *Appl. Catal. A*, 2001, 222 101-117.
12. J. D. Holbrey and K. R. Seddon, *Clean Prod. Proc.*, 1999, 1, 223-236.
13. R. D. Rogers and K. R. Seddon, *Science*, 2003, 302, 792-793.
14. T. Torimoto, T. Tsuda, K. Okazaki and S. Kuwabata, *Adv. Mater.*, 2010, 22, 1196-1221.
15. E. W. Castner Jr. and J. F. Wishart, *J. Chem. Phys.*, 2010, 132, 120901
16. F. Endres, *Phys. Chem. Chem. Phys.*, 2010, 12, 1648-1648.
17. H. Hamaguchi and R. Ozawa, in *Adv. Chem. Phys.*, ed. S. A. Rice, Wiley & Sons, 2005, vol. 131, pp. 85-104.
18. K. N. Marsh, J. A. Boxall and R. Lichtenthaler, *Fluid Phase Equil.*, 2004, 219 93-98.
19. C. Reichardt, *Green Chem.*, 2005, 7, 339-351.
20. R. D. Rogers and G. A. Voth, eds., "*Special Issue on Ionic Liquids*", *Account Chem. Res.*, 2007.
21. H. Weingartner, *Angew. Chem. Int. Ed.*, 2008, 47, 654-670.
22. A. Triolo, O. Russina, H.-J. Bleif and E. Di Cola, *J. Phys. Chem. B*, 2007, 111, 4641-4644.
23. R. Atkin and G. G. Warr, *J. Phys. Chem. B*, 2008, 112, 4164-4166.
24. K. Iwata, H. Okajima, S. Saha and H. Hamaguchi, *Acc. Chem. Res.*, 2007, 40, 1174-1181.
25. Y. Wang and G. A. Voth, *J. Am. Chem. Soc.*, 2005, 127, 12192-12193.
26. Y. Wang and G. A. Voth, *J. Phys. Chem. B*, 2006, 110, 18601-18608.
27. J. N. A. Canongia Lopes and A. H. Padua, *J. Phys. Chem. B*, 2006, 110, 3330-3335.
28. M. G. Del Popolo and G. A. Voth, *J. Phys. Chem. B*, 2004, 108, 1744-1752.
29. Z. Hu and C. J. Margulis, *Acc. Chem. Res.*, 2007, 40 1097-1105.
30. P. F. Barbara and W. Jarzaba, *Adv. Photochem.*, 1990, 15, 1-68.
31. H. Heitele, *Angew. Chem. Int. Ed. Engl.*, 1993, 32, 359-377.
32. R. A. Marcus, *Rev. Mod. Phys.*, 1993, 65, 599-610.
33. N. Mataga and H. Miyasaka, in *Advances in Chemical Physics*, eds. J. Jortner and M. Bixon, Wiley-Interscience, 1999, vol. 107, pp. 431-496.
34. W. P. de Boeij, M. S. Pshenichnikov and D. A. Wiersma, *J. Phys. Chem.*, 1996, 100, 11806-11823.
35. M. L. Horng, J. A. Gardecki, A. Papazyan and M. Maroncelli, *J. Phys. Chem.*, 1995, 99, 17311-17337.
36. T. Joo, J. Jia, J.-Y. Yu, M. J. Lang and G. R. Fleming, *J. Chem. Phys.*, 1996, 104, 6089-6108.
37. M. Maroncelli and G. R. Fleming, *J. Chem. Phys.*, 1987, 86, 6221-6239.
38. M. Maroncelli, J. Macinnis and G. R. Fleming, *Science* 1989, 243, 1674-1681.
39. S. J. Rosenthal, J. Jimenez and G. R. Fleming, *J. Mol. Liq.*, 1994, 60, 25-56.
40. S. J. Rosenthal, X. Xie, M. Du and G. R. Fleming, *J. Chem. Phys.*, 1991, 95, 4715-4718.
41. H. Sumi, *J. Chem. Phys.*, 1991, 95, 3334-3350.

42. H. Sumi and R. A. Marcus, *J. Chem. Phys.*, 1986, 84, 4894-4914.
43. H. Sumi and R. A. Marcus, *J. Chem. Phys.*, 1986, 84, 4272-4265.
44. D. Xiao, L. G. Hines Jr., S. Li, R. A. Bartsch and E. L. Quitevis, *J. Phys. Chem. B*, 2007, 113, 6426-6433.
45. A. Triolo, O. Russina, B. Fazio, G. B. Appetecchi, M. Carewska and S. Passerini, *J. Chem. Phys.*, 2009, 130, 164521
46. D. Xiao, L. G. Hines Jr., S. Li, R. A. Bartsch, E. L. Quitevis, O. Russina and A. Triolo, *J. Phys. Chem. B*, 2009, 113, 6426-6433.
47. A. Triolo, O. Russina, B. Fazio, R. Triolo and E. Di Cola, *Chem. Phys. Lett.*, 2008, 457, 362-365.
48. O. Russina, A. Triolo, L. Gontrani, R. Caminiti, D. Xiao, L. G. Hines Jr., R. A. Bartsch, E. L. Quitevis, N. Plechkova and K. R. Seddon, *J. Phys.: Condens. Matter*, 2009, 21 424121
49. J. N. A. C. Lopes and A. A. H. Padua, *J. Phys. Chem. B*, 2006, 110, 3330-3335.
50. Y. Wang, W. Jiang, T. Yan and G. A. Voth, *Acc. Chem. Res.*, 2007, 40, 1193-1199.
51. R. Hayes, S. Imberti, G. G. Warre and R. Atkina, *Phys. Chem. Chem. Phys.*, 2011, 13, 13544-13551.
52. A. Elaiwi, P. B. Hitchcock, K. R. Seddon, N. Srinivasan, T. Y.-M., T. Welton and J. A. Zora, *J. Chem Soc. Dalton Trans.*, 1995, 3467-3471.
53. A. Mele, C. D. Tran and S. H. De Paoli Lacerda, *Angew. Chem. Int. Ed.*, 2003, 42, 4364-4366.
54. M. G. Del Po'polo, R. M. Lynden-Bell and J. Kohanoff, *J. Phys. Chem. B*, 2005, 109, 5895-5902.
55. H. Sun, B. Qiao, D. Zhang and C. Liu, *J. Phys. Chem. A*, 2010, 114, 3990-3996.
56. Y. Zhou and M. Antonietti, *J. Am. Chem. Soc.*, 2003, 125, 14960-14961.
57. H. Itoh, K. Naka and Y. Chujo, *J. Am. Chem. Soc.*, 2004, 126, 3026-3027.
58. Y.-J. Zhu, W.-W. Wang, R.-J. Qi and X.-L. Hu, *Angew. Chem. Int. Ed.*, 2004, 116, 1434-1438.
59. Y. Qin, Y. Song, N. Sun, N. Zhao, M. i and L. Qi, *Chem. Mater.*, 2008, 20, 3965-3972.
60. J. Jiang, S.-H. Yu, W.-T. Yao, H. Ge and G.-Z. Zhang, *Chem. Mater.*, 2005, 17, 6094-6100.
61. Y. Zhou and M. Antonietti, *Chem. Mater.*, 2004, 16, 544-550.
62. M. Antonietti, D. Kuang, B. Smarsly and Y. Zhou, *Angew. Chem. Int. Ed.*, 2004, 43, 4988-4992.
63. K. Ueno, Y. Sano, A. Inaba, M. Kondoh and M. Watanabe, *J. Phys. Chem. B*, 2010, 114, 13095-13103.
64. K. Ueno and M. Watanabe, *Langmuir*, 2011, 27, 9105-9115.
65. M. Mezger, H. Schröder, H. Reichert, S. Schramm, J. S. Okasinski, S. Schöder, V. Honkimäki, M. Deutsch, B. M. Ocko, J. Ralston, M. Rohwerder, M. Stratmann and H. Dosch, *Science*, 2008, 322, 424-428.
66. R. Atkin and G. G. Warr, *J. Phys. Chem. C*, 2007, 111, 5162-5168.
67. R. Atkin, N. Borisenko, M. Drušchler, S. Z. El Abedin, F. Endres, R. Hayes, B. Huber and B. Roling, *Phys. Chem. Chem. Phys.*, 2011, 13, 6849-6857.
68. W. Jiang, Y. Wang and G. A. Voth, *J. Phys. Chem. B*, 2007, 111, 4812-4818.
69. F. Bardak, D. Xiao, L. G. Hines Jr., P. Son, R. A. Bartsch, E. L. Quitevis, P. Yang and G. A. Voth, *Chem. Phys. Chem.*, 2012, 13, 1687-1700.
70. J. D. Holbrey, W. M. Reichert, M. Nieuwenhuyzen, O. Sheppard, C. Hardacre and R. D. Rogers, *Chem. Commun.*, 2003, 476-477.
71. M. Deetlefs, C. Hardacre, M. Nieuwenhuyzen, O. Sheppard and A. K. Soper, *J. Phys. Chem. B*, 2005, 109, 1593-1598.
72. S. Patra and A. Samanta, *J. Phys. Chem. B*, 2012, 116, 12275-12283.
73. J. A. Ingram, R. S. Moog, N. Ito, R. Biswas and M. Maroncelli, *J. Phys. Chem. B*, 2003, 107, 5926-5932.
74. N. Ito, S. Arzhantsev, M. Heitz and M. Maroncelli, *J. Phys. Chem. B*, 2004, 108, 5771-5777.
75. A. M. Funston, T. A. Fadeeva, J. F. Wishart and E. W. Castner Jr, *J. Phys. Chem. B*, 2007, 111, 4963-4977.

76. K. Fruchey and M. D. Fayer, *J. Phys. Chem. B*, 2010, 114, 2840-2845.
77. D. C. Khara, J. P. Kumar, N. Mondal and A. Samanta, *J. Phys. Chem. B*, 2013, 117, 5156-5164.
78. D. C. Khara and A. Samanta, *Phys. Chem. Chem. Phys.*, 2010, 12, 7671-7677.
79. A. P. Demchenko, *Luminescence*, 2002, 17, 19-42.
80. P. K. Mandal, M. Sarkar and A. Samanta, *J. Phys. Chem. A*, 2004, 108, 9048-9053.
81. P. K. Mandal, A. Paul and A. Samanta, *J. Photochem. Photobio. A Chem.*, 2006, 182, 113-120.
82. A. Samanta, *J. Phys. Chem. B*, 2006, 110, 13704-13716.
83. H. Jin, X. Li and M. Maroncelli, *J. Phys. Chem. B*, 2007, 111, 13473-13478.
84. T. Shim, M. H. Lee, D. Kim and Y. Ouchi, *J. Phys. Chem. B*, 2008, 112, 1906-1912.
85. Z. Hu and C. J. Margulis, *PNAS*, 2006, 103, 831-836.
86. D. C. Khara and A. Samanta, *J. Phys. Chem. B*, 2012, 116, 13430-13438.
87. K. Suda, M. Terazima and Y. Kimura, *Chem. Phys. Lett.*, 2012, 531, 70-74.
88. S. Hayaki, Y. Kimura and H. Sato, *J. Phys. Chem. B*, 2013, 117, 6759-6767.
89. K. Suda, M. Terazima, H. Sato and Y. Kimura, *J. Phys. Chem. B*, 2013, 117, 12567-12582.
90. N. A. Smith and S. R. Meech, *Inter. Rev. Phys. Chem.*, 2002, 21, 75-100.
91. S. Ruhman, B. Kohler, A. G. Joly and K. A. Nelson, *IEEE J. Quant. Elect.*, 1988, 24, 470-481.
92. R. Righini, *Science*, 1993, 262, 1386-1390.
93. W. T. Lotshaw, D. McMorro, N. Thantu, J. S. Melinger and R. Kitchenham, *J. Raman Spec.*, 1995, 26, 571-583.
94. E. W. Castner Jr., J. F. Wishart and H. Shirota, *Acc. Chem. Res.*, 2007, 40, 1217-1227.
95. H. Shirota, A. M. Funston, J. F. Wishart and E. W. Castner Jr., *J. Chem. Phys.*, 2005, 122, 184512.
96. G. Giraud, C. M. Gordon, I. R. Dunkin and K. Wynne, *J. Chem. Phys.*, 2003, 119, 464-477.
97. D. A. Turton, J. Hunger, A. Stoppa, G. Hefter, A. Thoman, M. Walther, R. Buchner and K. Wynne, *J. Am. Chem. Soc.*, 2009, 131, 11140-11146.
98. B.-R. Hyun, S. V. Dzyuba, R. A. Bartsch and E. L. Quitevis, *J. Phys. Chem. A*, 2002, 106, 7579-7585.
99. D. Xiao, J. R. Rajian, A. Cady, S. Li, R. A. Bartsch and E. L. Quitevis, *J. Phys. Chem. B*, 2007, 111, 4669-4677.
100. C. Hardacre, J. D. Holbrey, S. E. J. McMath, D. T. Bowron and A. K. Soper, *J. Chem. Phys.*, 2003, 118, 273-278.
101. D. Xiao, J. R. Rajian, S. Li, R. A. Bartsch and E. L. Quitevis, *J. Phys. Chem. B*, 2006, 110, 16174-16178.
102. D. Xiao, J. R. Rajian, L. G. Hines Jr., S. Li, R. A. Bartsch and E. L. Quitevis, *J. Phys. Chem. B*, 2008, 112, 13316-13325.
103. H. Shirota and E. W. Castner Jr., *J. Phys. Chem. B*, 2005, 109, 21576-21585.
104. H. Shirota, K. Nishikawa and T. Ishida, *J. Phys. Chem. B*, 2009, 113, 9831-9839.
105. T. Ishida, K. Nishikawa and H. Shirota, *J. Phys. Chem. B*, 2009, 113, 9840-9851.
106. H. Shirota, H. Fukazawa, T. Fujisawa and J. F. Wishart, *J. Phys. Chem. B*, 2010, 114, 9400-9412.
107. N. Mataga, H. Yao, T. Okada and W. Rettig, *J. Phys. Chem.*, 1989, 93, 3383-3386.
108. E. Z. Lippert, *Elektrochem. Ber. Bunsenges. Phys. Chem.*, 1957, 61, 962-975.
109. N. Mataga, Y. Kaifu and M. Koizumi, *Bull. Chem. Soc. Jap.*, 1956, 29, 465-470.
110. N. Mataga, Y. Kaifu and M. Koizumi, *Bull. Chem. Soc. Jap.*, 1955, 28, 690-691.
111. M. Maroncelli, X.-X. Zhang, M. Liang, D. Roy and N. P. Ernsting, *Faraday Discuss.*, 2012, 154, 409-424.
112. A. Samanta, *J. Phys. Chem. Lett.*, 2010, 1, 1557-1562.
113. S. Pandey, S. N. Baker, S. Pandey and G. A. Baker, *J. Fluoresc.*, 2012, 1313-1343.
114. P. K. Mandal, S. Saha, R. Karmakar and A. Samanta, *Current Science*, 2006, 90, 301-310.
115. E. W. Castner Jr., C. J. Margulis, M. Maroncelli and J. F. Wishart, *Annu. Rev. Phys. Chem.*, 2011, 62, 85-105.

116. R. Karmakar and A. Samanta, *J. Phys. Chem. A*, 2002, 106, 4447-4452.
117. R. Karmakar and A. Samanta, *J. Phys. Chem. A*, 2003, 107, 7340-7346.
118. P. K. Mandal and A. Samanta, *J. Phys. Chem. B*, 2005, 109, 15172-15177.
119. P. K. Mandal, A. Paul and A. Samanta, *Res. Chem. Intermed.*, 2005, 31, 575-583.
120. D. Seth, A. Chakraborty, P. Setua and N. Sarkar, *J. Phys. Chem. B*, 2007, 111, 4781-4787.
121. A. Paul and A. Samanta, *J. Phys. Chem. B*, 2007, 111, 4724-4731.
122. S. Arzhantsev, H. Jin, G. A. Baker and M. Maroncelli, *J. Phys. Chem. B*, 2007, 111, 4978-4989.
123. H. Jin, G. A. Baker, S. Arzhantsev, J. Dong and M. Maroncelli, *J. Phys. Chem. B*, 2007, 111, 7291-7301.
124. H. Jin, B. O'Hare, J. Dong, S. Arzhantsev, G. A. Baker, J. F. Wishart, A. J. Benesi and M. Maroncelli, *J. Phys. Chem. B*, 2008, 112, 81-92.
125. X.-X. Zhang, M. Liang, N. P. Ernsting and M. Maroncelli, *J. Phys. Chem. B*, 2013, 117, 4291-4304.
126. M. A. Kahlow, W. Jarz̄ba, T. P. DuBruil and P. F. Barbara, *Rev. Sci. Instrum.*, 1988, 59, 1098-1109.
127. J. Shah, *IEEE J. of Quant. Elect.*, 1988, 24, 276-288.
128. S. Kinoshita, H. Ozawa, Y. Kanematsu, I. Tanaka, N. Sugimoto and S. Fujiwara, *Rev. Sci. Instrum.*, 2000, 71, 3317-3322.
129. J. Takeda, K. Nakajima and S. Kurita, *Phys. Rev. B*, 2000, 62, 10083-10087.
130. H. Rhee and T. Joo, *Opt. Lett.*, 2005, 30, 96-98.
131. S. Arzhantsev, H. Jin, N. Ito and M. Maroncelli, *Chem. Phys. Lett.*, 2006, 417, 524-529.
132. B. Lang, G. Angulo and E. Vauthey, *J. Phys. Chem. A*, 2006, 110, 7028-7034.
133. M. Cho, J.-Y. Yu, T. Joo, Y. Nagasawa, S. A. Passino and G. R. Fleming, *J. Phys. Chem.*, 1996, 100, 11944-11953.
134. Y. Shim, M. Y. Choi and H. J. Kim, *J. Chem. Phys.*, 2005, 122, 044511
135. M. N. Kobrak, *J. Chem. Phys.*, 2006, 125, 064502
136. Y. Shim, D. Jeong, S. Manjari, M. Y. Choi and H. J. Kim, *Acc. Chem. Res.*, 2007, 40, 1130-1137.
137. S. Arzhantsev, N. Ito, M. Heitz and M. Maroncelli, *Chem. Phys. Lett.*, 2003, 381, 278-286.
138. X.-X. Zhang, M. Liang, N. P. Ernsting and M. Maroncelli, *J. Phys. Chem. Lett.*, 2013, 4, 1205-1210.
139. R. Richert, *Chem. Phys. Lett.*, 1990, 171, 222-228.
140. R. Richert, F. Stickel, R. S. Fee and M. Maroncelli, *Chem. Phys. Lett.*, 1994, 229, 302-308.
141. M. Maroncelli, *J. Chem. Phys.*, 1997, 106, 1545-1555.
142. X. Song and D. Chandler, *J. Chem. Phys.*, 1998, 108, 2594-2600.
143. M. Sajadi, T. Oberhuber, S. A. Kovalenko, M. Mosquera, B. Dick and N. P. Ernsting, *J. Phys. Chem. A*, 2009, 113, 44-55.
144. S. Daschakraborty, T. Pal and R. Biswas, *J. Chem. Phys.*, 2013, 139, 164503.
145. P. Sen, S. Ghosh, S. K. Mondal, K. Sahu, D. Roy, K. Bhattacharyya and K. Tominaga, *Chem. Asian. J.*, 2006, 1-2, 188-194.
146. Y. Nagasawa, M. Cho and G. R. Fleming, *Faraday Discuss.*, 1997, 108, 23-34.
147. G. R. Fleming and M. Cho, *Annu. Rev. Phys. Chem.*, 1996, 47, 109-134.
148. S. A. Passino, Y. Nagasawa and G. R. Fleming, *J. Chem. Phys.*, 1997, 107, 6094-6108.
149. S. A. Passino, Y. Nagasawa, T. Joo and G. R. Fleming, *J. Phys. Chem. A*, 1997, 101, 725-731.
150. Y. Nagasawa, R. Mukai, K. Mori, M. Muramatsu and H. Miyasaka, *Chem. Phys. Lett.*, 2009, 482, 263-268.
151. T. Joo and A. C. Albrecht, *Chem. Phys.*, 1993, 176, 233-247.
152. S. Mukamel, *Principles of Nonlinear Optical Spectroscopy*, Oxford University Press, New York, 1995.
153. Y. Nagasawa, J.-Y. Yu and G. R. Fleming, *J. Chem. Phys.*, 1998, 109, 6175-6183.
154. Y. Nagasawa, S. A. Passino, T. Joo and G. R. Fleming, *J. Chem. Phys.*, 1997, 106, 4840-4852.

155. X. Yang, T. E. Dykstra and G. D. Scholes, *Phys. Rev. B*, 2005, 71, 045203.
156. E. A. Gibson, Z. Shen and R. Jimenez, *Chem. Phys. Lett.*, 2009, 473, 330-335
157. R. Jimenez, G. Salazar, J. Yin, T. Joo and F. E. Romesberg, *PNAS*, 2004, 101, 3803-3808.
158. H. Lee, Y.-C. Cheng and G. R. Fleming, *Science*, 2007, 316, 1467-1465.
159. M.-L. Groot, J.-Y. Yu, R. Agarwal, J. R. Norris and G. R. Fleming, *J. Phys. Chem. B*, 1998, 102, 5923-5931.
160. R. Agarwal, M. Yang, Q.-H. Xu and G. R. Fleming, *J. Chem. Phys. B*, 2001, 105, 1887-1894.
161. J.-Y. Yu, Y. Nagasawa, R. van Grondelle and G. R. Fleming, *Chem. Phys. Lett.*, 1997, 280 404-410.
162. M. Muramatsu, Y. Nagasawa and H. Miyasaka, *J. Phys. Chem. A*, 2011, 115, 3886-3894.
163. Y. Nagasawa, Y. Mori, Y. Nakagawa, H. Miyasaka and T. Okada, *J. Phys. Chem. B*, 2005, 109, 11946-11952.
164. Y. Nagasawa, K. Seike, T. Muromoto and T. Okada, *J. Phys. Chem. A*, 2003, 107, 2431-2441.
165. C. J. Bardeen, G. Cerullo and C. V. Shank, *Chem. Phys. Lett.*, 1997, 280, 127-133.
166. C. J. Bardeen, S. J. Rosenthal and C. V. Shank, *J. Phys. Chem. A*, 1999, 103, 10506-10516.
167. S. Daschakraborty and R. Biswas, *J. Chem. Phys.*, 2012, 137, 114501
168. S. Mukamel, *Annu. Rev. Phys. Chem.*, 1990, 41, 647-681.
169. Y. J. Yan and S. Mukamel, *J. Chem. Phys.*, 1991, 94, 179-190.
170. H. K. Kashyap and R. Biswas, *J. Phys. Chem. B*, 2010, 114, 254-268.
171. R. A. Marcus and N. Sutin, *Biochim.t Biophys. Acta - Reviews on Bioenergetics*, 1985, 811 265-322.
172. M. D. Newton and N. Sutin, *Annu. Rev. Phys. Chem.*, 1984, 35, 437-480.
173. J. Jortner and M. Bixon, *J. Chern. Phys.*, 1988, 88, 167-170.
174. J. Ulstrup and J. Jortner, *J. Chem. Phys.*, 1975, 63, 4358-4368.
175. B. Bagchi, G. R. Fleming and D. W. Oxtoby, *J. Chem. Phys.*, 1983, 78, 7375-7385.
176. Y. Nagasawa, A. P. Yartsev, K. Tominaga, P. B. Bisht, A. E. Johnson and K. Yoshihara, *J. Phys. Chem.*, 1995, 99, 653-662.
177. Y. Nagasawa, A. P. Yartsev, K. Tominaga, A. E. Johnson and K. Yoshihara, *J. Chem. Phys.*, 1994, 101, 5717-5726.
178. K. Yoshihara, K. Tominaga and Y. Nagasawa, *Bull. Chem. Soc. Jpn.*, 1995, 68, 697-712.
179. F. Pöllinger, C. Musewald, H. Heitele, M. E. Michel-Beyerle, C. Anders, M. Futscher, G. Voit and H. A. Staab, *Ber. Bunsenges. Phys. Chem.*, 1996, 100, 2076-2080.
180. T. Häberle, J. Hirsch, F. Pöllinger, H. Heitele and M. E. Michel-Beyerle, *J. Phys. Chem.*, 1996, 100 18269-18274.
181. C. Khurmi and M. A. Berg, *J. Phys. Chem. Lett.*, 2010, 1, 161-164.
182. K. Sahu, S. J. Kern and B. M. A., *J. Phys. Chem. A*, 2011, 115, 7984-7993.
183. Y. Shim and H. J. Kim, *J. Phys. Chem. B*, 2007, 111, 4510-4519.
184. Y. Shim and H. J. Kim, *J. Phys. Chem. B*, 2009, 113, 12964-12972.
185. J. V. Lockard and M. R. Wasielewski, *J. Phys. Chem. B*, 2007, 111, 11638-11641.
186. H. Y. Lee, J. B. Issa, S. S. Isied, E. W. Castner Jr., Y. Pan, C. L. Hussey, K. S. Lee and J. F. Wishart, *J. Phys. Chem. C*, 2012, 116, 5197-5208.
187. K. Santhosh and A. Samanta, *Chem. Phys. Chem*, 2012, 13, 1956-1961.
188. A. Paul and A. Samanta, *J. Phys. Chem. B*, 2007, 111, 1957-1962.
189. A. K. Das, T. Mondal, S. S. Mojumdar and K. Bhattacharyya, *J. Phys. Chem. B*, 2011, 115, 4680-4688.
190. M. Liang, A. Kaintz, G. A. Baker and M. Maroncelli, *J. Phys. Chem. B*, 2012, 116, 1370-1384.
191. D. W. Anthon and J. H. Clark, *J. Phys. Chem.*, 1987, 91, 3530-3536.
192. T. J. Kang, W. Jarzeba, P. F. Barbara and T. Fonseca, *Chem. Phys.*, 1990, 149, 81-95.
193. S. A. Kovalenko, J. L. Perez Lustres, N. P. Ernsting and W. Rettig, *J. Phys. Chem. A*, 2003, 107, 10228-10232.
194. T. Takaya, H. Hamaguchi, H. Kuroda and K. Iwata, *Chem. Phys. Lett.*, 2004, 399, 210-214.

195. T. Takaya, S. Saha, H. Hamaguchi, M. Sarkar, A. Samanta and K. Iwata, *J. Phys. Chem. A*, 2006, 110, 4291-4295.
196. Y. Tsuboi, T. Kumagai, M. Shimizu, A. Itaya, G. Schweitzer, F. C. De Schryver, T. Asahi, H. Masuhara and H. Miyasaka, *J. Phys. Chem. A*, 2002, 106, 2067-2073.
197. Y. Nagasawa, T. Itoh, M. Yasuda, Y. Ishibashi, S. Ito and H. Miyasaka, *J. Phys. Chem. B*, 2008, 112, 15758-15765.
198. Y. Nagasawa, A. Oishi, T. Itoh, M. Yasuda, M. Muramatsu, Y. Ishibashi, S. Ito and H. Miyasaka, *J. Phys. Chem. C*, 2009, 113, 11868-11876.
199. H. Shizuka, Y. Ishii and T. Morita, *Chem. Phys. Lett.*, 1977, 51, 40-44.
200. M. Mac, J. Najbar and J. Wirz, *J. Photochem. Photobio. A Chem.*, 1995, 88, 93-104.
201. G. Grabner, K. Rechthaler and G. Kohler, *J. Phys. Chem. A*, 1998, 102, 689-696.
202. X. Li, M. Liang, A. Chakraborty, M. Kondo and M. Maroncelli, *J. Phys. Chem. B*, 2011, 115, 6592-6607.
203. K. Tominaga, G. C. Walker, T. J. Kang, P. F. Barbara and T. Fonseca, *J. Phys. Chem.*, 1991, 95, 10485-10492.
204. K. Tominaga, G. C. Walker, W. Jarzqba and P. F. Barbara, *J. Phys. Chem.*, 1991, 95, 10475-10485.
205. N. Nakashima, M. Murakawa and M. Mataga, *Bull. Chem. Soc. Jpn.*, 1976, 49, 854-858.
206. M. Jurczok, T. Gustavsson, J.-C. Mialocq and W. Rettig, *Chem. Phys. Lett.*, 2001, 344, 357-366.
207. D. C. Khara, A. Paul, K. Santhosh and A. Samantha, *J. Chem. Sci.*, 2009, 121, 309-315.
208. M. Muramatsu, S. Morishima, T. Katayama, S. Ito, Y. Nagasawa and H. Miyasaka, *J. Sol. Chem.*, 2014, In press.
209. M. Muramatsu, T. Katayama, S. Ito, Y. Nagasawa, D. Matsuo, Y. Suzuma, L. Peng, A. Orita, J. Otera and H. Miyasaka, *Photochem. Photobiol. Sci.*, 2013, 12, 1885-1894.

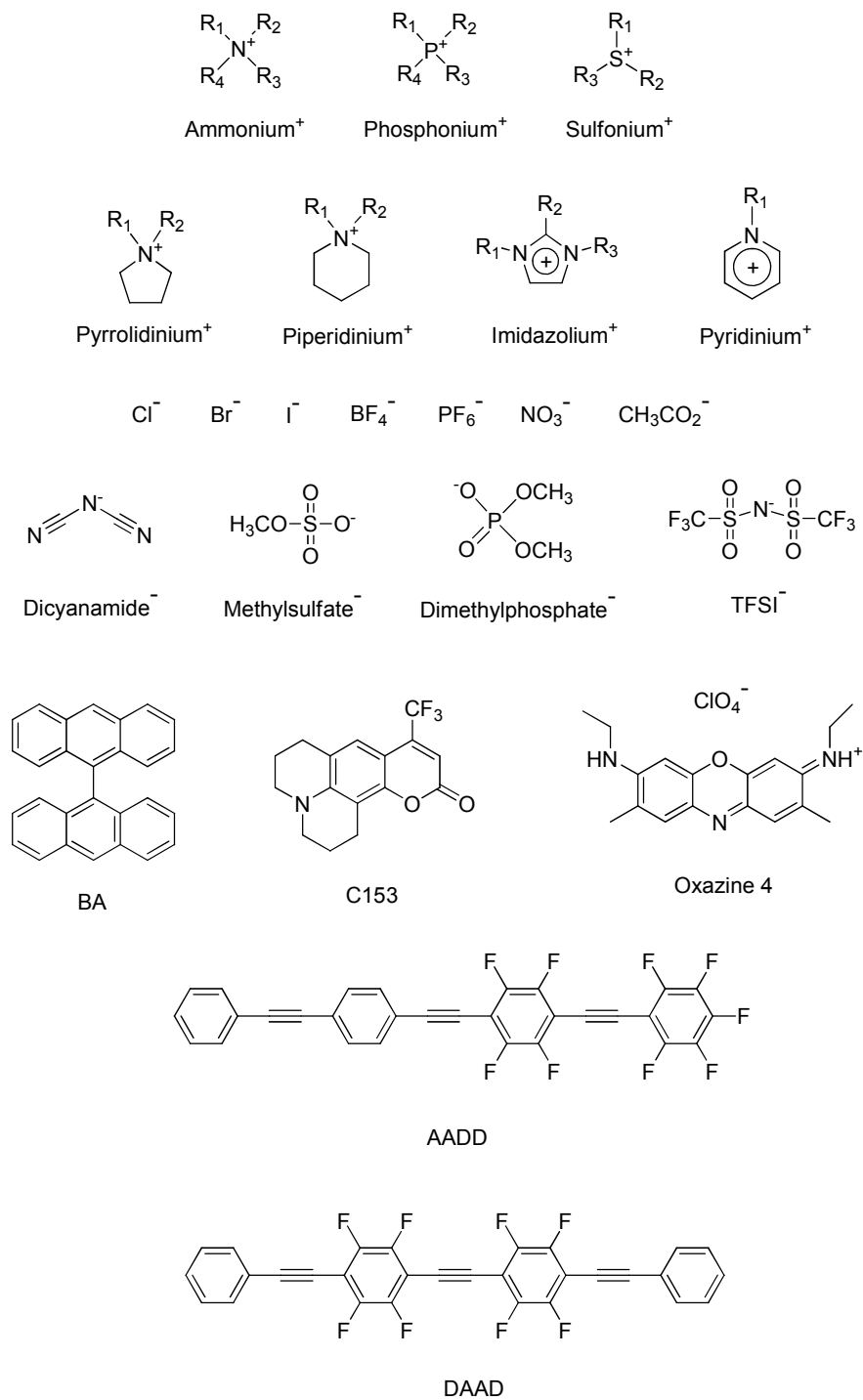


Figure 1. Molecular structures of typical ionic liquid (IL) cations and anions and solute molecules introduced in this article.

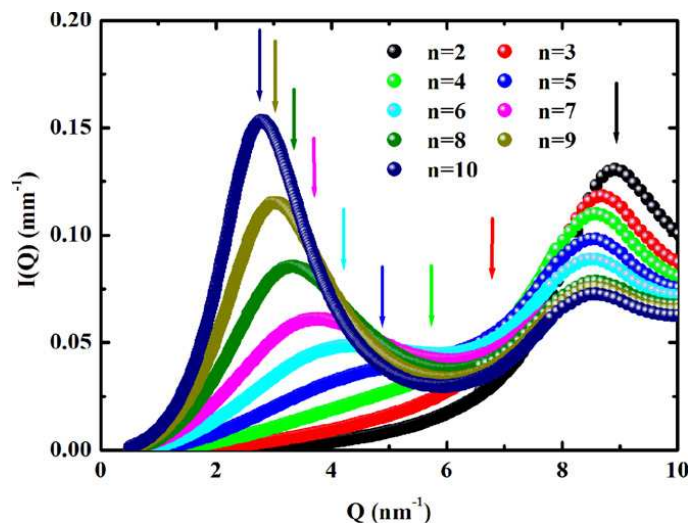


Figure 2. Low- Q portion of the small-wide-angle X-ray scattering data for the 1,3-dialkylimidazolium bis(trifluoromethanesulfonyl)amide series with $n = 2-10$ at room temperature. The arrows indicate the position of the peak at low Q that strongly depends both in amplitude and position on n . Reprinted with permission from ref.⁴⁸ Copyright (2009) IOP Publishing Ltd.

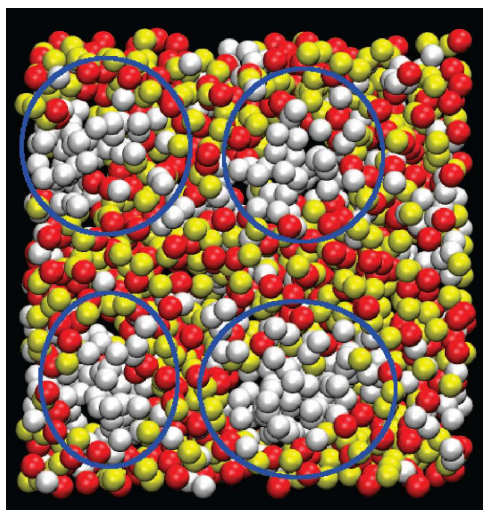


Figure 3. The heterogeneous tail aggregation of IL observed by molecular dynamics simulation. The white and yellow spheres represent the tail and head of the cation and the red spheres represent the anions. The ellipses in blue illustrate the approximate positions of the nonpolar domains. Reprinted with permission from ref. ⁵⁰. Copyright (2007) American Chemical Society.

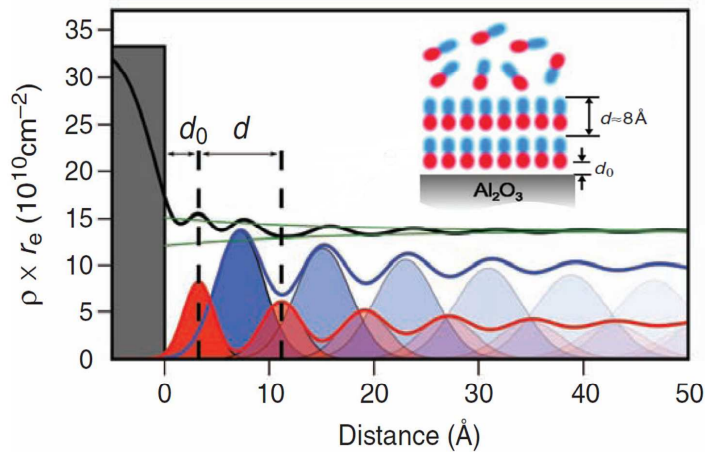


Figure 4. The cation (red), anion (blue), and total (black) electron density profiles at the 1-*n*-butyl-1-methylpyrrolidinium tris(pentafluoroethyl)trifluorophosphate-sapphire interface (temperature: -15°C) obtained from fitting the high-energy x-ray reflectivity data. d_0 is the distance between the substrate's surface and the center of the first ion layer, while d is the layer spacing ($\sim 8 \text{ \AA}$). Inset shows a layering arrangement of correlated ions on a sapphire surface with double-layer stacking. Reproduced from ref. ⁶⁵ with permission. Copyright (2008) Science.

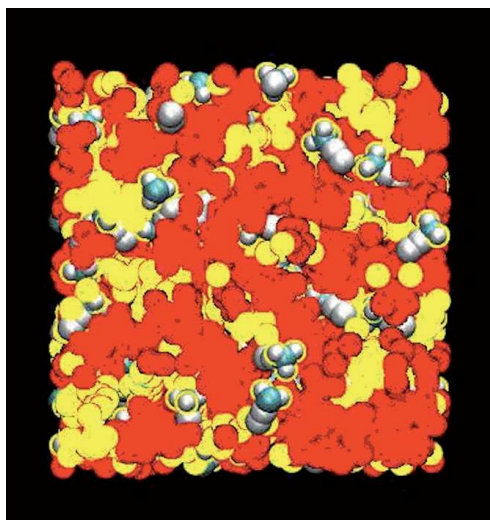


Figure 5. MD simulation snapshot of the nanostructural organization in 50 mol% acetonitrile in IL, 1-pentyl-3-methylimidazolium bis[(trifluoromethane)sulfonyl]amide, with the polar domains colored red, the nonpolar domains colored yellow, and the acetonitrile molecules represented by space-filling structures. Reprinted from ref. ⁶⁹ with permission. Copyright (2012) Wiley-VCH Verlag GmbH & Co. KGaA.

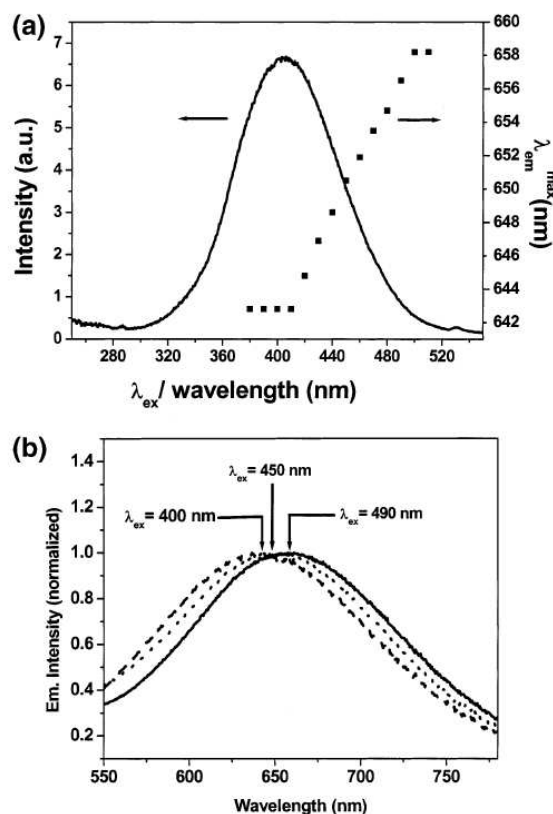


Figure 6. (a) Maximum emission wavelength plotted against excitation wavelength for 2-amino-7-nitrofluorene (ANF) in BmimBF₄ (filled squares) superimposed on the excitation spectrum. (b) Normalized fluorescence spectra of ANF in BmimBF₄ as a function of excitation wavelength. Reprinted from ref. ⁸⁰ with permission. Copyright (2004) American Chemical Society.

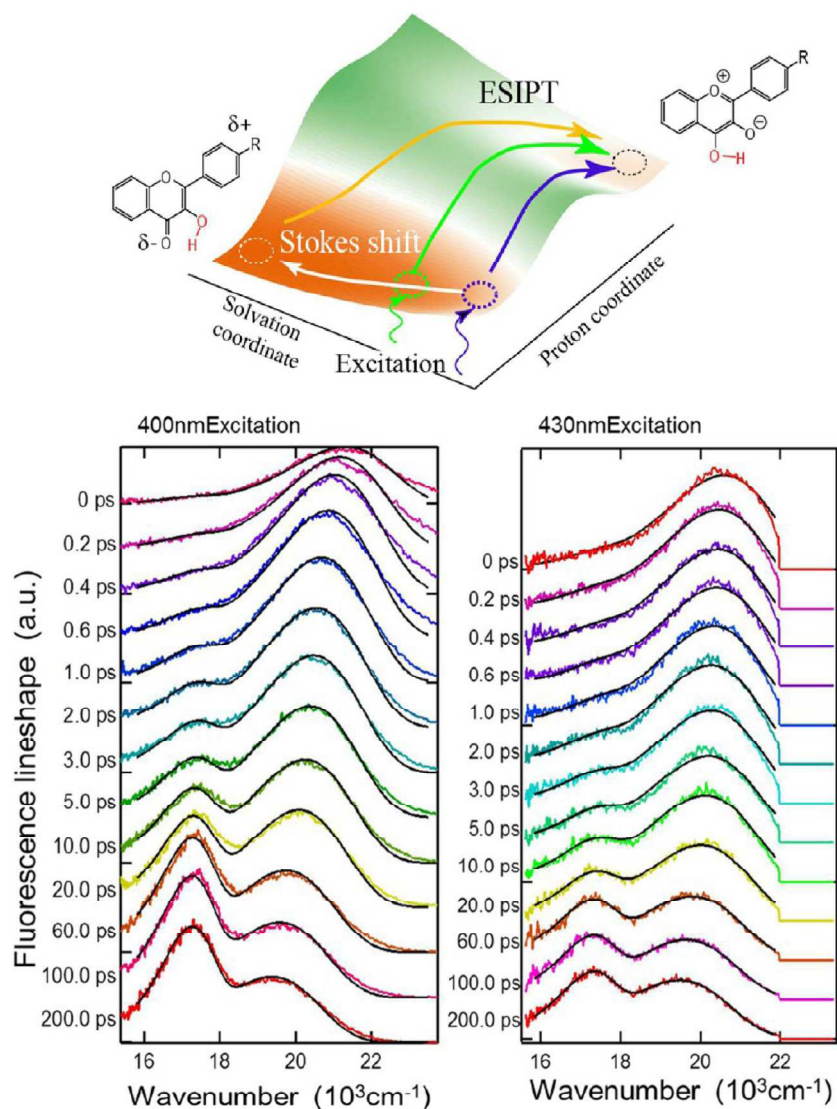


Figure 7. Top: Schematic illustration of the excited state energy surface and reaction pathways at different excitation wavelengths of DEAHF in ILs. Bottom: Time-resolved fluorescence line shapes of DEAHF in BmimPF₆ obtained at 400 nm (bottom left) and 430 nm (bottom right) excitations. The black solid lines show the spectral fitting results. Reproduced from ref. ⁸⁹ with permission. Copyright (2013) American Chemical Society.

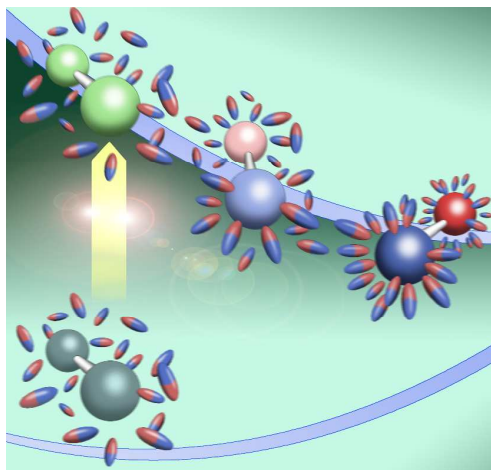


Figure 8. Schematic illustration of solvation process against a newly formed electric dipole moment in the excited state for the case of normal polar solvent. Reproduced from the cover of Noboru Mataga Festschrift, *J. Phys. Chem. A* 106(10) (2002) with permission. Copyright (2002) American Chemical Society.

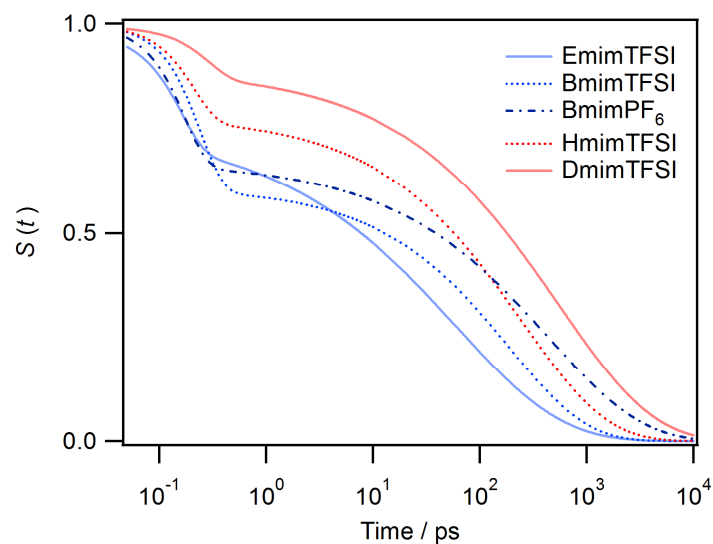


Figure 9. Solvation correlation function, $S(t)$, for typical imidazolium IL with 1-ethyl-, 1-butyl-, 1-hexyl-, and 1-decyl-3-methylimidazolium (Emim^+ , Bmim^+ , Hmim^+ , and Dmim^+) cations and bis(trifluoromethylsulfonyl)imide (TFSI) and hexafluorophosphate (PF_6^-) anions.¹²⁵

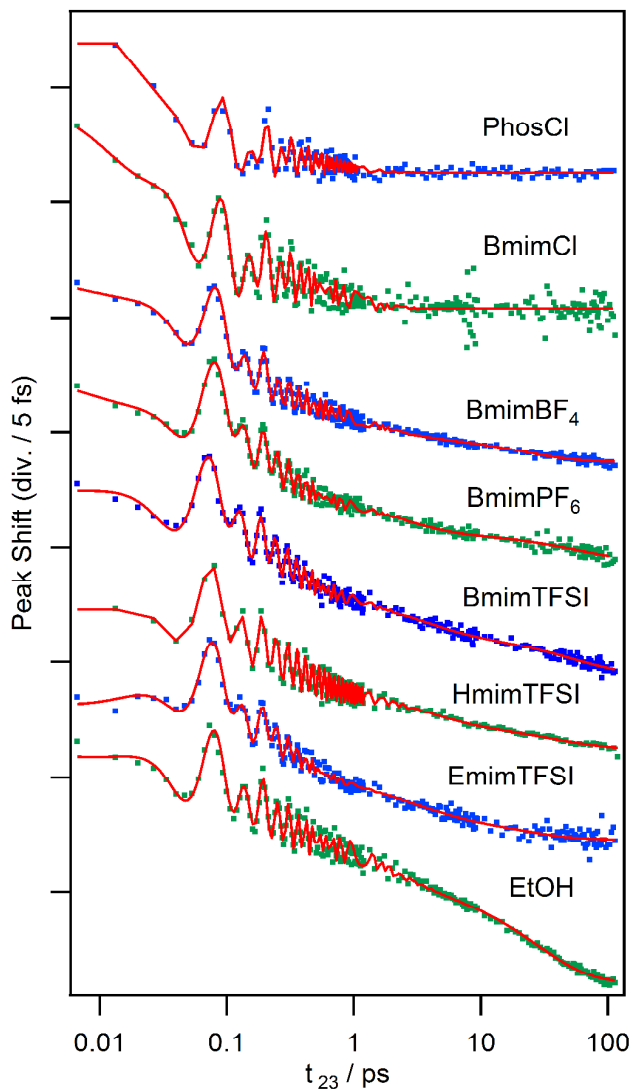


Figure 10. 3PEPS signal of Ox4 in various ILs and in ethanol (EtOH). The signals are shifted vertically to avoid overlap. ¹⁶²PhosCl stands for trihexyltetradecylphosphonium chloride.

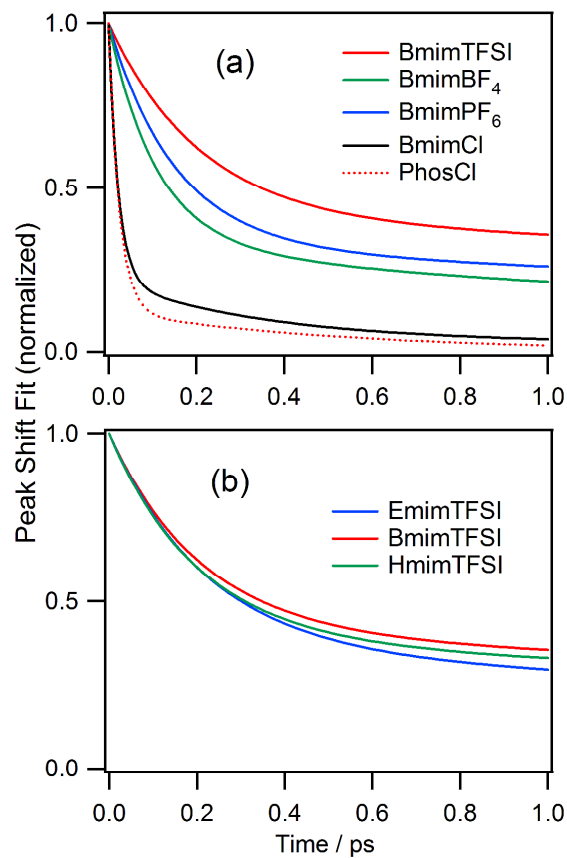


Figure 11. (a) Anion and (b) cation dependences of the ultrafast part (≤ 1.0 ps) of the normalized fitting curve, which corresponds to the "inertial" component of solvation, obtained from 3PEPS signals in ILs. Asymptotic peak shift and intramolecular vibrations are neglected.¹⁶²

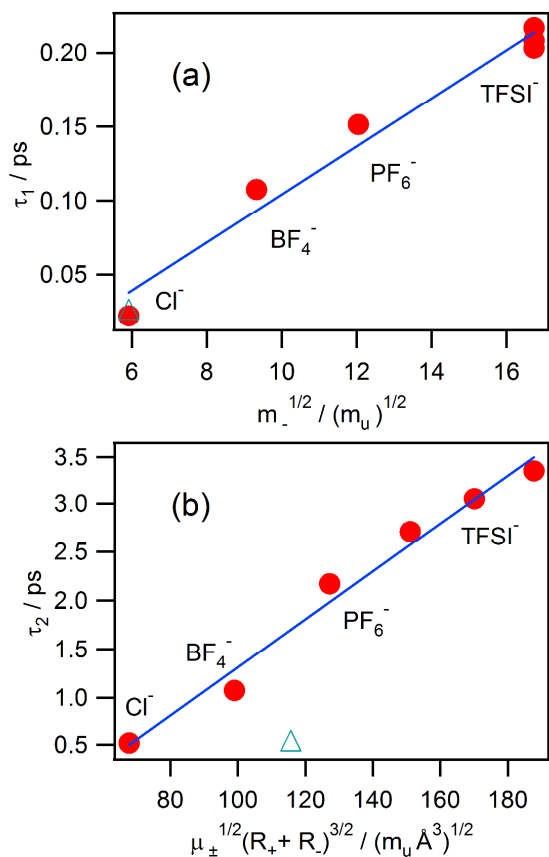


Figure 12. The time constants (a) τ_1 and (b) τ_2 for the initial ultrafast and the second peak shifts, respectively, plotted against the square root of the anion mass and the inertial factor $\sqrt{\mu_{\pm}(R_+ + R_-)^3}$, respectively. The blue line is the result of the least-squares fit to the plots. Triangle is the point for PhosCl^{162} .

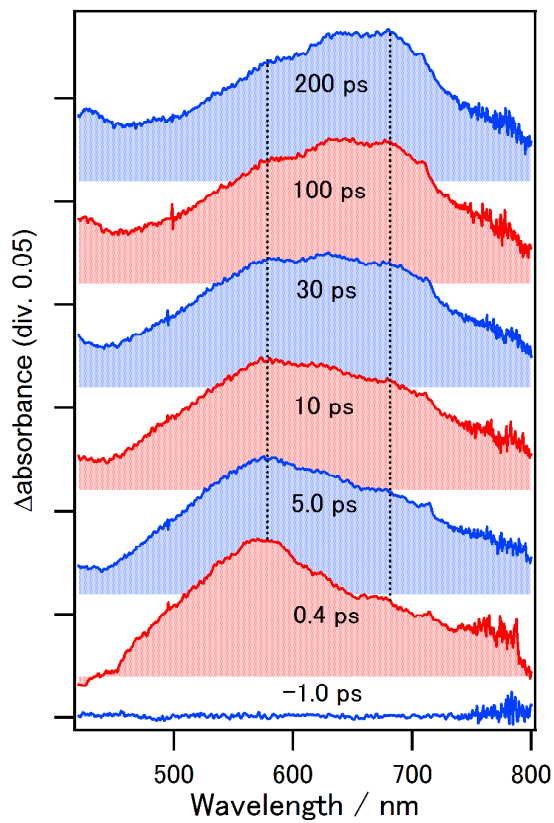


Figure 13. Femtosecond transient absorption (TA) spectra of 9,9'-bianthryl in BmimTFSI excited at 400 nm.¹⁹⁷

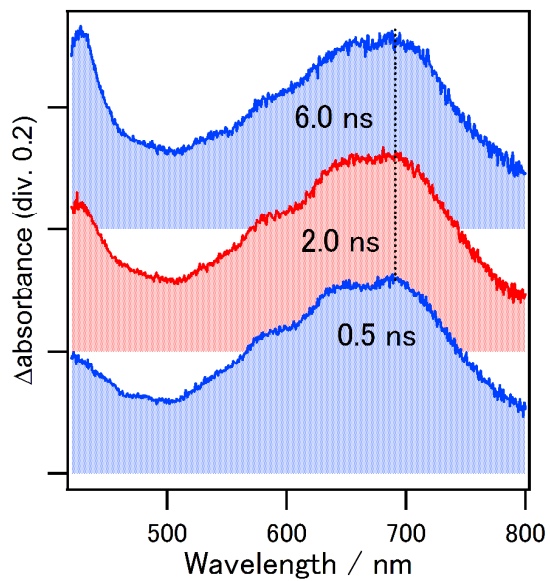


Figure 14. Picosecond TA spectra of 9,9'-bianthryl in BmimTFSI excited at 355 nm.¹⁹⁷

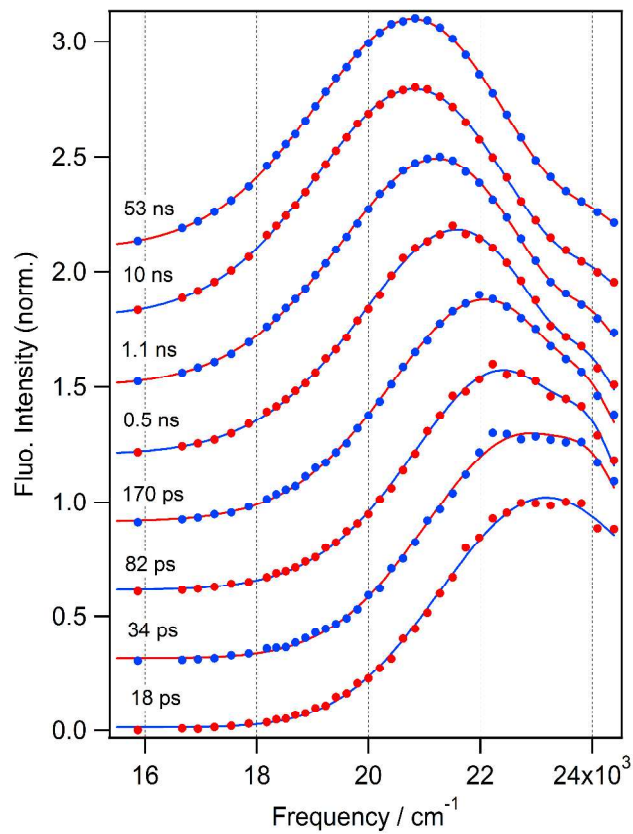


Figure 15. Time-resolved fluorescence (TRF) spectra of BA in BmimTFSI measured at various time delays, 18, 34, 82, 170 ps, 0.5, 1.1, 10, and 53 ns, respectively.¹⁹⁸

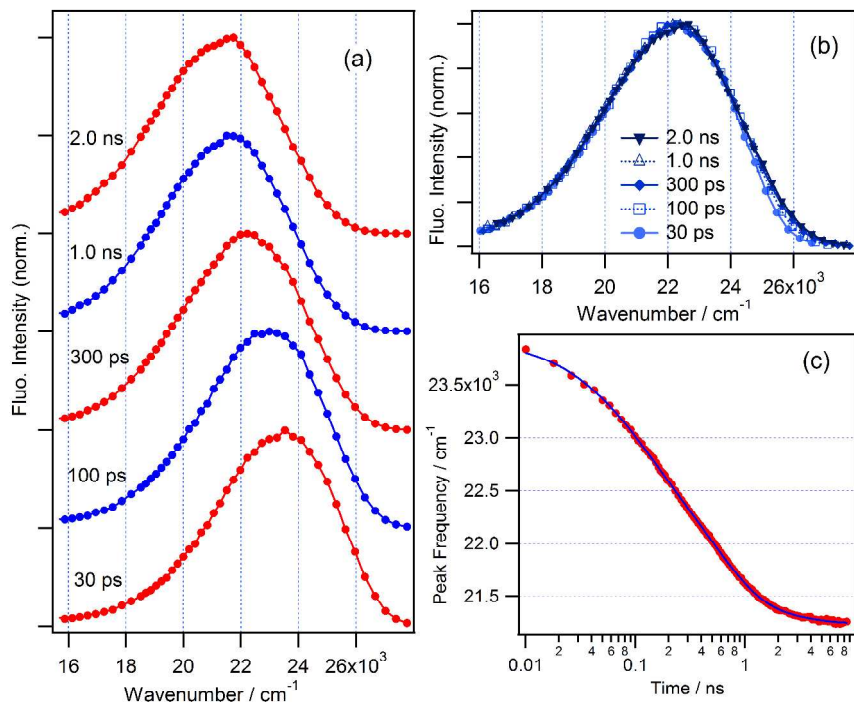


Figure 16. (a) Normalized TRF spectra of AADD in BmimTFSI, excited with a 350-nm laser pulse. (b) Normalized TRF spectra at 30, 100, 300 ps, and 1.0, 2.0 ns. The spectra were horizontally shifted to overlap with the one at 300 ps. (c) Time profile of the fluorescence maximum (red circle) and the multiexponential fitting curve (blue solid curve).²⁰⁹

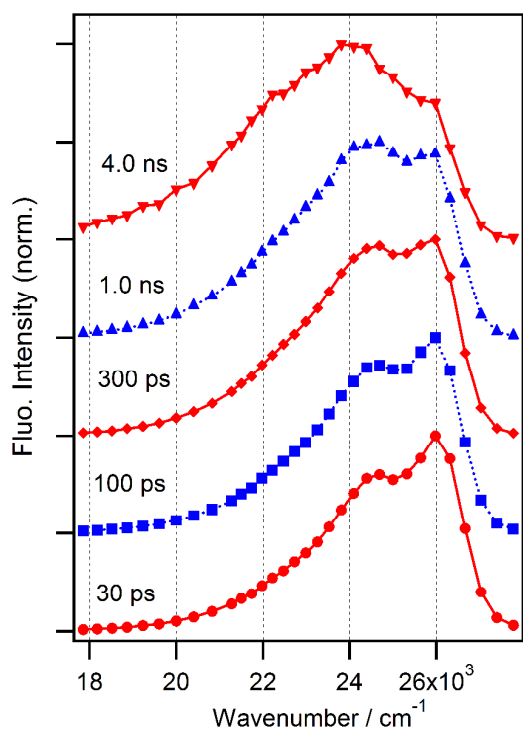


Figure 17. Normalized TRF spectra of DAAD in BmimTFSI, excited with a 350-nm laser pulse.²⁰⁹